Middle Pleistocene glaciation in Patagonia dated by cosmogenic-nuclide measurements on outwash gravels

Middle Pleistocene glaciation in Patagonia dated by cosmogenic-nuclide measurements on outwash gravels

Andrew S. Hein*, Nicholas R. J. Hulton, Tibor J. Dunai, Christoph Schnabel, Michael R. Kaplan, Mark Naylor and Sheng Xu

*Corresponding Author

School of Geosciences
University of Edinburgh
Drummond Street
Edinburgh, UK
EH8 9XP

Cite As: Hein, A, Hulton, N, Dunai, T, Schnabel, C, Kaplan, MR, Naylor, M & Xu, S 2009, 'Middle Pleistocene glaciation in Patagonia dated by cosmogenic-nuclide measurements on outwash gravels' *Earth and Planetary Science Letters*, vol 286, no. 1-2, pp. 184-197.

DOI: 10.1016/j.epsl.2009.06.026

Abstract

The well-preserved glacial record in Argentine Patagonia offers a ~1 Ma archive of terrestrial climate extremes in southern South America. These glacial deposits remain largely undated beyond the range of radiocarbon dating at ca. 40 ka. Dating old glacial deposits (> several 10^5 a) by cosmogenic surface exposure methods is problematic because of the uncertainty in moraine degradation and boulder erosion rates. Here, we show that cobbles on outwash terraces can reliably date 'old' glacial deposits in the Lago Pueyrredón valley, 47.5º S, Argentina. Favorable environmental conditions (e.g., aridity and strong winds) have enabled continuous surface exposure of cobbles and preservation of outwash terraces. The data demonstrate that nuclide inheritance is negligible and we therefore use the oldest surface cobbles to date the deposit. ^{10}Be concentrations in outwash cobbles reveal a major glacial advance at ca. 260 ka, concurrent with Marine Isotope Stage 8 (MIS 8) and dust peaks in Antarctic ice cores. A ^{10}Be concentration depth-profile in the outwash terrace supports the age and suggests a low terrace erosion rate of ca. 0.5 mm ka^{-1}. We compare these data to exposure ages obtained from associated moraines and find that surface boulders under-estimate the age of the glaciation by ~100 ka; thus the oldest boulders in this area do not date closely moraine deposition. The ^{10}Be concentration in moraine cobbles help to constrain moraine degradation rates. These data together with constraints from measured ^{26}Al/^{10}Be ratios suggest that all moraine boulders were likely exhumed after original deposition. We determine the local Last Glacial Maximum (LGM) occurred at ~27 – 25 ka, consistent with the maximum LGM in other parts of Patagonia.

Keywords: Cosmogenic nuclide surface exposure dating; Marine Isotope Stage 8; Glacial chronology; Southern South America; Beryllium-10; Last Glacial Maximum.

1. INTRODUCTION

The aim of this research is to establish a more reliable method of dating pre-Last Glacial Maximum (LGM) ice limits using cosmogenic surface exposure dating methods on glacial outwash terrace material as opposed to moraine boulders. Specifically, this approach is used to date the well-preserved sequence of Quaternary ice limits in Argentine Patagonia. These limits are well documented (e.g., Caldenius, 1932; Clapperton, 1993; Flint and Fidalgo, 1964; Mercer, 1976; Rabassa and Clapperton, 1990; Singer et al., 2004) but have proved difficult to date thus far. Our approach is to avoid the problems that inadvertently arise from dating boulders that have been exhumed as a moraine degrades. We achieve this by sampling fluvial rounded cobbles from stable outwash terrace surfaces that are stratigraphically associated with the moraines. Applicability of the method is dependent on three principal factors: First, linking outwash abandonment to a specific glacial event; second, on there being low nuclide inheritance in outwash sediment; and third, that there is no post-depositional burial, mixing or removal of the terrace sediment. We argue that these favorable conditions are met in parts of Argentine Patagonia and may occur in other arid and aeolian active environments elsewhere. In this paper, we compare ^{10}Be exposure ages obtained from (1) moraine boulders with (2) moraine cobbles and (3) outwash terrace cobbles of the same glacial event in the Lago Pueyrredón valley, 47.5º S, Argentina. The palaeoclimatic significance of the new chronology developed in this study will be addressed in future publications.

1.1 Patagonian glacial history and the age gap

Well-dated moraines older than the LGM are sparse in Patagonia reflecting a lack of dateable material and the limit of radiocarbon dating beyond ~40 ka. Most outlet valleys in arid Argentine Patagonia contain four to five groups of moraines and associated outwash terraces (Caldenius, 1932; Clapperton, 1993; Kaplan et al., 2009). The deposits range from the innermost LGM (~25 ka) deposits to the outermost 'Greatest Patagonian Glaciation' deposits dated at ~1.1 Ma (Meglioli, 1992; Mercer, 1976; Rabassa and Clapperton, 1990; Rabassa et al., 2000; Singer et al., 2004; Ton-That et al., 1999). In many cases, these end members often provide the only age framework for intermediate deposits (i.e. between LGM time and ~1.1 Ma). Recently, Kaplan et al. (2005) demonstrated the potential of cosmogenic surface exposure methods to fill these gaps when they identified a glacial advance around 140 – 150 ka (MIS 6) and at least one prior to 200 ka at Lago Buenos Aires (LBA), 46.5º S, Argentina. Despite good moraine preservation and low boulder erosion rates (~1.4 mm ka^{-1}), the wide scatter in boulder exposure ages made interpretation of the age of older moraines challenging.

1.2 Exposure dating of old moraines

Boulders on old moraines (i.e., older than several 10^5 a) frequently yield wide scatter in exposure ages that is commonly attributed to boulder erosion rate uncertainty and exhumation (e.g., Benson et al., 2004; Briner et al., 2005; Kaplan et al., 2007; Kaplan et al., 2005; Owen et al., 2006; Phillips et al., 1990; Schäfer et al., 2008; Shanahan and Zreda, 2000). Poorly constrained (or non steady-state) boulder erosion rates are known to affect significantly the accuracy of older exposure ages, even with relatively low rates of 1 mm ka^{-1} (Gillespie and Bierman, 1995). Moraine degradation leads to

erroneously young boulder exposure ages (Hallet and Putkonen, 1994; Phillips et al., 1990; Putkonen and Swanson, 2003; Zreda et al., 1994) and therefore the oldest boulder can be used to date the deposit (cf. Zreda and Phillips, 1995). However, the rate of degradation is site-specific and is rarely quantifiable. Without additional constraints, the amount of moraine degradation and its effect on boulder exposure ages remains difficult to assess and is not routinely considered. Recent model findings suggest degradation may be ubiquitous and high (Putkonen et al., 2008; Putkonen and O'Neal, 2006); thus even the oldest boulder ages may not date closely moraine deposition. The increasing uncertainty on exhumation and erosion rates with increasing moraine ages often limits the results to minimum limiting ages.

1.3 Exposure dating of outwash terraces

Glacial outwash terraces can often be directly linked to moraines that mark former ice limits. They are frequently better preserved than moraines owing to their low-gradient surfaces which are less prone to degradation. The surfaces may contain fluvial rounded cobbles and original surface channel morphology that, providing the terrace has not been reactivated post-depositionally, indicate minimal clast erosion or exhumation since deposition. This suggests outwash terraces may be feasible for exposure dating. However, small clasts on flat surfaces are more prone to burial (e.g., seasonal snow cover, soil, loess) and mixing (e.g., cryo- or bio-turbation, up-freezing, overturning) than large moraine boulders, which together with potential aeolian inflation or deflation of the terrace surface, can complicate the exposure history (Gosse and Phillips, 2001).

Fluvial terraces associated with glacial events have been dated in previous studies (e.g., Brocard et al., 2003; Chadwick et al., 1997; Hancock et al., 1999; Phillips et al., 1997; Repka et al., 1997; Schildgen et al., 2002). Surface clasts may contain inherited nuclides obtained prior to mobilization and during clast transport to the site of final deposition. Methods have been developed to quantify the average nuclide inheritance in a fluvial deposit (e.g., Anderson et al., 1996; Hancock et al., 1999; Repka et al., 1997), but nuclide inheritance in individual clasts can vary significantly around this mean (e.g., Hancock et al., 1999). Zentmire et al. (1999) measured ^{10}Be concentrations in cobbles of modern day glacial outwash. These samples contained negligible inherited nuclides which they attribute to both sub-glacial erosion and shielding by the overriding glacier prior to deposition (Gosse and Phillips, 2001). If both nuclide inheritance and clast mixing can be shown to be negligible, and ^{26}Al/^{10}Be ratios indicate no prolonged burial, then individual surface clasts from outwash terraces could be suitable targets for dating old glacial events in regions where boulder exhumation and erosion is an issue. With this in mind, we targeted a well-preserved moraine and outwash sequence in Patagonia.

2. LAGO PUEYRREDÓN VALLEY, 47.5º S, ARGENTINA

The Lago Pueyrredón (LP) valley (Figure 1) was a major outlet of former Patagonian ice sheets and the glacial record is exceptionally well-preserved (Figure 2). It is located in close proximity to the dated long-term glacial record at Lago Buenos Aires (LBA).

2.1 Geology

The LP valley is a west – east trending glacial depression separating the Meseta del Lago Buenos Aires to the north and the Mesetas Belgrano and Olnie to the south (Figure 2). The nearest granitic rocks are within the San Lorenzo Plutonic Complex, about 80 km from the innermost moraines (Suárez and De La Cruz, 2001). The nearest sources for quartz cobbles are veins in the Eastern Andes Metamorphic Complex located 65 km west of the innermost moraines; thus clast transport distances of the sampled lithologies are large.

Based on the pioneering work of Caldenius (1932), four major glacial units are distinguished over a range of 40 km with the outermost deposits situated more than 350 meters higher than the innermost (Figure 2). Each unit is separated by escarpments of up to 100 meters. This over-deepened valley shares a peculiarity in drainage common throughout Patagonia; lakes and rivers on the eastern mountain front drain to the Pacific Ocean, except during glacial times when the continuous N – S oriented ice sheet forced drainage eastward to the Atlantic Ocean (Figure 1a). This unique hydrologic condition is partly responsible for the exceptional preservation of the deposits. Pre-LGM outwash terraces are also well-preserved because the trend in ice extent has in general decreased over time (Kaplan et al., 2009). During glacial maxima, melt-water discharged directly onto broad outwash plains until ice began to retreat and pro-glacial lakes formed, dammed by terminal moraines. This caused rivers to incise in response to the decreased sediment load (cf. Chorley et al., 1984), thereby abandoning outwash terraces. Pro-glacial lakes are evident by the preserved shorelines below the Hatcher and Río Blanco moraines (Figure 2), these eventually drained westward when the Río Baker depression became ice free (Figure 1a; Mercer,

1976). We infer that outwash terraces stabilized shortly after glacial maximum conditions.

2.2 Climate

The current climate in the study area is semi-arid with precipitation levels of 200 mm a^{-1} and strong and persistent winds[1]. Annual snow cover is thin and short-lived (Local land owners, personal communication) and models predict increased aridity during glacial times (Hulton et al., 2002). Also, strong winds quickly removed ash deposited by the 1991 eruption of Volcán Hudson in Chile (Inbar et al., 1995) and an increase in the vigor of atmospheric circulation during glacial times (Petit et al., 1999) would likely lead to higher wind velocities. Wind has observably been a dominant agent of erosion with boulders commonly exhibiting ventifacts and flutings (Figure 3a). Cobbles and pebbles on the Hatcher outwash terrace often exhibit rock varnish on ventifacts (Figure 3b) suggesting aeolian erosion was not recent. We propose that aeolian erosion was episodic in nature, occurring during glacial maxima when outwash plains were active, devoid of vegetation and debris was available for entrainment by wind (cf. Sugden et al., 2009). Therefore, we assume that post-depositional shielding by annual snow cover, loess or other deposits is limited today and during glacial times, even on flat outwash terraces.

2.3 Existing glacial chronology

[1] NCEP/NCAR reanalysis; www.cdc.noaa.gov/ncep_reanalysis/

The glacial chronology at Lago Pueyrredón previously was poorly developed. There is no direct chronology for the deposits at Lago Pueyrredón. The only dates come from three sources: First, Sylwan et al. (1991) measured magnetic polarity in glacial sediments and found that part of the outermost mapped Caracoles unit was deposited during the reversed Matuyama chron at more than 780 ka (Singer and Pringle, 1996); second, Mercer (1976; 1982) dated peat in the former melt-water drainage near the entrance to the Cañadón de Caracoles at ~11.8 ^{14}C ka (Figure 2), providing a minimum age for the Río Blanco moraines (Wenzens, 2005); third, Wenzens (2005) dated a mollusc shell from a lake deposit at the foot of the Cañadón de Caracoles escarpment, inside the limit of the Hatcher moraines. The date of ~17.2 ^{14}C ka led Wenzens (2005) to conclude that the Hatcher moraines were deposited during the LGM as proposed by Caldenius (1932), and the Río Blanco moraines must therefore be late glacial in age. However, the lack of a firm chronology makes correlation to deposits in nearby valleys tentative and subject to debate (Kaplan et al., 2006; Wenzens, 2006). Additional age limits were estimated (initially, before results were obtained) based on correlation of Caldenius' (1932) mapping with deposits dated at LBA (Figure 1b). Four major moraine groups are identified in both valleys. At LBA, cosmogenic dating of the Fenix and Moreno I-II moraines indicated they are LGM (~16-23 ka; Douglass et al., 2006; Kaplan et al., 2004), and MIS 6 in age (~140-150 ka; Kaplan et al., 2005). Steadily older glacial events are represented through the mid Quaternary (~1.1 Ma) based on limiting ^{40}Ar/^{39}Ar ages (Singer et al., 2004).

3. APPROACH AND METHODOLOGY

To assess whether old glacial deposits can be dated more reliably using outwash terrace cobbles as opposed to moraine boulders, we compare ^{10}Be and ^{26}Al exposure ages obtained from both sample types on the Hatcher unit, assumed to be pre-LGM in age (Figure 1b). In addition, we sampled the outermost moraine and associated outwash terrace of the younger (est. LGM) Río Blanco unit as a 'geologic blank' allowing a test of the following fundamental assumptions: (1) terraces stabilized shortly after moraine deposition; (2) nuclide inheritance is low; (3) post-depositional shielding is minimal; and (4) terrace sediment are not mixed post-depositionally. If valid, exposure ages from all samples of the younger Río Blanco unit should be indistinguishable and date the timing of the event.

For the Hatcher moraines, degradation and erosion is expected to complicate interpretation of boulder exposure ages. To address the relative magnitude of these processes, we sampled moraine cobbles. Because negligible rock surface erosion can be inferred from the preservation of smooth, rounded cobble surfaces, lower nuclide concentrations in cobbles relative to boulders will likely be the result of shielding by the moraine matrix, provided that ^{26}Al/^{10}Be ratios are not consistent with prolonged burial. Thus moraine cobble nuclide concentrations can help to estimate the amount of degradation. On the Hatcher outwash terrace we additionally sampled a ^{10}Be concentration depth-profile to exploit the depth dependency of cosmogenic nuclide production. These data provide further constraints on the average nuclide inheritance, deposition age and exposure history of the outwash sediment while allowing checks on sediment mixing that could affect exposure ages obtained from individual surface clasts.

3.1 Sampling

3.1.1 Sampling criteria and methods

Moraine boulders were sampled with hammer and chisel following established protocols (e.g., Gosse and Phillips, 2001). We preferentially sampled the top few centimeters of large (> 1 meter) stable boulders (granite) on or near moraine crests showing minimal evidence of surface erosion (Figure 3c). Moraine and outwash cobbles of quartz (5 – 25 cm long axis) were sampled to obtain a sufficient quartz yield and because monomineralic quartz clasts are resistant to weathering. These were collected whole from well-preserved moraine crests (Figure 3c) and from terrace surfaces away from moraines and scarps. The samples were later crushed whole (small cobbles/pebbles) or after cutting to an appropriate thickness, and subsequently sieved to obtain the 250 – 710 μm fraction.

The depth profile was sampled in a small quarry along Route 40 (Figure 4) at a location where the surrounding surface appeared undisturbed by the excavation. The deposit is composed of cobbles to coarse sands throughout (Figure 3e). Soils are poorly developed in the top 10 – 15 cm (<30% fines at top of profile) and about 40% of the deposit is cemented by pedogenic carbonate at ~30 – 100 cm depth. The bulk density was estimated based on grain size distribution at 2.57 g cm^{-3} with an assumed error of ± 0.1 g cm^{-3} (cf. Hancock et al., 1999). This is based on the observation that 75% of the deposit contains grain sizes larger than coarse sands with a clast density of 2.7 g cm^{-3} (30% porosity), an interstitial sand density of 2.7 g cm^{-3} (30% porosity) and a pedogenic carbonate density of 2.4 g cm^{-3} occupying 40% of the remaining

interstitial space. Eight samples were collected at depths ranging from 10 – 150 cm. Each sample was composed of ten to fifty quartz pebbles (2 – 4 cm) that were amalgamated following Repka et al. (1997). We use the thickness of the largest clast in each sample as measure of the uncertainty of depth (Table 1).

3.1.2 Sample location

Sample locations are shown in Figures 2 and 4. We sampled the outermost moraine crest and, where possible, from outwash terraces that can be directly mapped to the corresponding dated moraine. Both moraine crests are generally sparsely vegetated with desert pavements (gravels – cobbles) formed at some locations (Figure 3d). Most moraine boulders are ventifacted while rounded moraine cobbles are more often not; neither show rock varnish. The Río Blanco moraines were sampled on the south side of the valley where they are best preserved. The moraines are hummocky but largely continuous with ~20 – 25 meters of relief and slopes of ~20º. The Hatcher moraines are situated 100 m above the Río Blanco outwash and were sampled in more lateral positions on both sides of the valley (over 30 km apart). Moraine relief ranges from 20 – 30 m above the associated outwash terrace to the east (~18º slopes) and from 40 – 50 m above an inter-moraine depression to the west (19º – 25º slopes).

The Río Blanco and Hatcher outwash terraces occupy ~240 km^2 and 325 km^2 in area, respectively. The surfaces dip gently eastward at < 0.5º and converge at the entrance to, and above the Cañadón de Caracoles (Figure 2). Both terraces are composed of gravels and coarse sands with local concentrations of cobbles and pebbles. These small lag deposits are not underlain by fine sediments (i.e., they are not inflationary

desert pavements). Vegetation cover is sparse. Shallow surface channels (1 – 3 m) are well-preserved with clear braiding patterns visible; these often grade to recessional moraine positions. Río Blanco outwash was sampled at a location where it could be directly traced to the dated moraine. The Hatcher outwash was sampled at two locations on the northern terrace (Figure 4). Here, three minor (1 – 3m) terrace levels grade to a common base level and can be traced to Hatcher recessional ice limits further west. The first sample site (S1) can be directly mapped to the dated moraine. The second site (S2), which is also the location of the depth-profile, occupies a similar stratigraphic position but is located ~8 km from the dated moraine.

3.2 Depth-profile exposure model optimization

The depth-profile allows defining the age and erosion rate of the terrace surface and testing of several underlying assumptions. In-situ ^{10}Be production in the upper few meters of the Earth's surface is dominated by high-energy neutron spallation reactions that decrease exponentially with attenuation of the secondary cosmic ray flux at depth. Assuming the Hatcher terrace material was deposited in a single event and remained stable with a single continuous erosion rate, we would expect to observe a smooth exponential decrease of nuclide concentration within the profile that can be described by an appropriately parameterized model. The expected ^{10}Be concentration at depth (z) can be modeled for any given terrace age (t), erosion rate (ε_{terr}), overburden density (ρ) and inherited nuclide concentration (N_{inh}) using the following analytical approximation for production at depth in a steadily eroding deposit (after Granger and Smith, 2000):

$$
\begin{aligned}
N &= N_{inh}e^{-t\lambda} \\
&+ \left[P_n e^{-\rho z/\Lambda} / \left(\lambda + \rho\varepsilon_{terr}/\Lambda\right)\right]\left[1 - e^{-t\left(\lambda+\rho\varepsilon_{terr}/\Lambda\right)}\right] \\
&+ \left[P_{\mu 1} e^{-\rho z/L_1} / \left(\lambda + \rho\varepsilon_{terr}/L_1\right)\right]\left[1 - e^{-t\left(\lambda+\rho\varepsilon_{terr}/L_1\right)}\right] \\
&+ \left[P_{\mu 2} e^{-\rho z/L_2} / \left(\lambda + \rho\varepsilon_{terr}/L_2\right)\right]\left[1 - e^{-t\left(\lambda+\rho\varepsilon_{terr}/L_2\right)}\right] \\
&+ \left[P_{\mu^{fast}} e^{-\rho z/L_3} / \left(\lambda + \rho\varepsilon_{terr}/L_3\right)\right]\left[1 - e^{-t\left(\lambda+\rho\varepsilon_{terr}/L_3\right)}\right]
\end{aligned}
\qquad (1)
$$

where N is the ^{10}Be concentration, N_{inh} is the inherited ^{10}Be concentration, λ is the ^{10}Be radioactive decay constant (5.1x10^{-7} a^{-1})(Nishiizumi et al., 2007), P_n, $P_{\mu 1}$, $P_{\mu 2}$ and P_μ^{fast} are production rates due to neutron spallation, negative muon capture ($_{\mu 1}$, $_{\mu 2}$) and fast muon reactions, while Λ (160 g cm^{-2}), L_1 (738.6 g cm^{-2}), L_2 (2688 g cm^{-2}) and L_3 (4360 g cm^{-2}) are the respective attenuations lengths provided by Granger and Smith (2000). Production rates for each reaction were calculated as a fraction of the total surface production rate with f_n = 0.9724, $f_{\mu 1}$ = 0.0186, $f_{\mu 2}$ = 0.004 and f_μ^{fast} = 0.005 integrated over the sample thickness (*Pn* only; cf. Vermeesch, 2007). The time-averaged surface production rate value is 8.22 atoms ^{10}Be g^{-1} a^{-1} (Dunai, 2001)(see supplementary material).

Assuming the terrace deposit experienced a simple exposure history at a constant erosion rate, there should be only one combination of exposure age, terrace erosion rate, overburden density and nuclide inheritance that best fits all the measured data points in the profile. A forward model can be used to obtain the parameters that minimize the difference between the predicted and observed nuclide concentrations. In this study, we use the sum of chi-squared ($\Sigma\chi^2$) for the exposure model optimization. Because the bulk density was estimated in the field (Section 3.1.1), we solve for the exposure duration (t), erosion rate (ε_{terr}) and nuclide inheritance (N_{inh})

that best fit the measured profile data and their associated analytical uncertainties (σ_i), such that:

$$\sum \chi^2 \equiv \sum_{i=1}^{N} \left(\frac{y_i - y(t, \varepsilon_{terr}, N_{inh})}{\sigma_i} \right)^2 \quad (2)$$

where y_i is the measured ^{10}Be concentration at a particular sample depth and $y(t,\varepsilon_{terr},N_{inh})$ is the modeled ^{10}Be concentration at that depth for any given $(t,\varepsilon_{terr},N_{inh})$ solution. The analytical uncertainties (σ_i) include both sample and blank ^{10}Be/^{9}Be uncertainties and a 2% carrier addition/sample mass uncertainty. For a quantitative assessment of the model's ability to describe the measured data, we assess the 'goodness of fit' to the data using the reduced chi-squared (χ_r^2) value. The χ_r^2 is the sum of chi-squared divided by the degrees of freedom, and this value should approach 1 if the fitting function describes the data well (cf. Bevington and Robinson, 2003, p. 194). The exposure model therefore allows a best estimate of the terrace age, erosion rate and average nuclide inheritance by the sum of chi-squared, and allows us to quantify (χ_r^2) how well the data fit the underlying model.

3.3 Exposure age calculations

The ^{10}Be and ^{26}Al exposure ages were calculated with the CRONUS-Earth exposure age calculator (version 2.2 ;Balco et al., 2008)[2] which implements the revised ^{10}Be standardization and half-life (1.36 Ma) of Nishiizumi et al. (2007). Exposure ages are reported based on the Dunai (2001) scaling model; these differ by up to ~5%

[2] (http://hess.ess.washington.edu/math/index_dev.html)

depending on the choice of alternative scaling model. The calculator uses sample thickness (Table 2) and density (assumed 2.7 g cm^3) to standardize nuclide concentrations to the rock surface. Topographic shielding was measured but is negligible (scaling factor <0.9998). We apply no correction for snow or vegetation shielding. No erosion rate correction is applied to the cobble data, but an erosion rate of 1.4 mm ka^{-1} is used to document this effect on boulder exposure ages; this value was derived by Kaplan et al. (2005) for boulders on the Telken moraines at LBA, 60km to the north. Sample elevations were converted to air pressures for input into the calculator; we assumed a standard atmosphere for the elevation-pressure relationship. The local sea-level (SL) pressure and temperature (1009.3 hPa/285K)[3] was used to convert elevations to air pressures for samples of the younger Río Blanco unit. We used a lower SL pressure for the conversion of the older Hatcher samples as described below.

The time-averaged ^{10}Be and ^{26}Al production rates near Lago Pueyrredón have been estimated to be 5% and 11% higher than for standard atmospheric conditions by two independent studies that infer a low pressure anomaly during glacial times (cf. Ackert et al., 2003; Staiger et al., 2007). Following Staiger et al. (2007), we increase ^{10}Be and ^{26}Al production rates by ~5% for samples on the older Hatcher unit (for discussion see supplementary material). We note that, however, that the conclusions of this paper are not sensitive to the choice of correction used. The 5% higher production rate was implemented within the exposure age calculator by artificially lowering the air pressure at the sampled locations, thereby increasing the production rates. Specifically, we lowered the SL pressure that was used in the conversion of

[3] NCEP-NCAR reanalysis; www.cdc.noaa.gov/ncep_reanalysis/

sample elevations to sample air pressures; the present day SL pressure (1009.3 hPa) was lowered to 1002.3 hPa. The lower SL pressure reduces the calculated sample air pressures, and thereby increases the time-averaged production rate derived through the calculator by approximately 5% when compared against the value obtained from a calculation based on the present day SL pressure.

4. RESULTS

The analytical results are presented in Tables 1 and 2 and Figures 4 – 7. Samples were prepared at the University of Edinburgh's Cosmogenic Isotope Laboratory. Information on the chemical procedure is provided in the supplementary material. The AMS measurements were conducted at the AMS-facility at SUERC. Measurements are normalized to the NIST SRM-4325 Be standard material with a revised (Nishiizumi et al., 2007) nominal $^{10}Be/^{9}Be$ ratio of 2.79×10^{-11}, and the Purdue Z92-0222 Al standard material with a nominal $^{27}Al/^{26}Al$ ratio of 4.11×10^{-11} which agrees with the Al standard material of Nishiizumi et al. (2004). The $^{26}Al/^{10}Be$ production rate ratio is 6.69. Samples are corrected for the number of ^{10}Be and ^{26}Al atoms in their associated blanks. Blanks (n = 8) were spiked with 250 µg ^{9}Be carrier and 1.5 mg ^{27}Al carrier. Samples were spiked with 250 µg ^{9}Be carrier and up to 1.5 mg ^{27}Al carrier (the latter value varied depending on the native Al-content of the sample). For each batch of 7 samples one blank was processed. The corresponding combined process and carrier blanks range between 115,000 ± 18,000 atoms ^{10}Be and 290,000 ± 40,000 atoms ^{10}Be (< 3% of total ^{10}Be atoms in sample; $0.9 – 1.7 \times 10^{-14}$ [$^{10}Be/^{9}Be$]); and between 61,000 ± 12,000 atoms ^{26}Al and 190,000 ± 57,000 atoms ^{26}Al (< 1% of total ^{26}Al atoms in sample; $2.6 – 3.8 \times 10^{-15}$ [$^{27}Al/^{26}Al$]). Sample and

blank $^{10}Be/^{9}Be$ and $^{27}Al/^{26}Al$ analytical uncertainties and a 2% carrier addition uncertainty and 5% stable ^{27}Al measurement (ICP-OES) uncertainty are propagated into the 1σ analytical uncertainty for nuclide concentrations (Tables 1 and 2). Throughout the text, if not stated otherwise, uncertainties are reported as 1σ. Analytical uncertainties are reported, except for means where we report the standard deviation of the population.

4.1 Río Blanco unit

The ^{10}Be boulder exposure ages from the outermost moraine crest range from 25.4 – 32.2 ka (no erosion). The oldest boulder (BC07-8) falls outside 2σ analytical uncertainty of the remaining population. Excluding this sample, the range is from 25 – 27 ka and the three ages overlap within error. The arithmetic mean age is 26.0 ± 1.0 ka, or 26.8 ± 1.0 including a correction for erosion (sect. 3.3). The three outwash cobbles yield ^{10}Be exposure ages of 24.3 ± 0.8 ka, 24.6 ± 0.8 ka and 25.3 ± 0.7 ka and thus are indistinguishable within uncertainties. The mean outwash cobble age (24.7 ± 0.5 ka) is indistinguishable from the boulder mean at 2σ. The low sample variability (σ = 0.5 ka) of outwash cobbles and indistinguishable ages from moraine boulders confirms our initial assumptions (1-4; see section 3.0).

4.2 Hatcher unit

4.2.1 Moraine samples

The four moraine boulder samples yield a wide range of ^{10}Be exposure ages from 107.4 – 190 ka with a mean of 149.3 ± 37.6 ka (w/erosion; Figure 5). The high standard deviation highlights the significant variability often observed in 'old' moraine boulder ages. The age range normalized to the oldest boulder (0.38) is typical for moraines (Putkonen and Swanson, 2003). The oldest boulder age (BC07-3) assuming no erosion is 152.8 ± 4.4 ka and corresponds to the tallest boulder sampled on the Hatcher moraines (2m; Figure 3c). The ^{26}Al/^{10}Be ratios are consistent with relatively simple exposure histories without prolonged burial.

The moraine cobble ^{10}Be exposure ages range from 41.7 – 57.9 ka with a mean of 48.3 ± 6.3 ka (Table 2, Figure 5). The young ages are not thought to be caused by post-depositional burial and re-exposure based on our assessment of the geomorphic environment (Section 2.2). In addition, the ^{26}Al/^{10}Be ratios are also consistent with a simple exposure history without prolonged burial. Based on this, we infer that low nuclide concentrations (i.e., young exposure ages) are the result of moraine degradation, which appears to be similar at both sample localities > 30 km apart.

4.2.2 ^{10}Be concentration depth-profile

The depth-profile data is presented in Table 1 and Figures 6 and 7. Figure 7 shows that the ^{10}Be concentration decreases exponentially with depth; consistent with post-deposition production in a stable terrace and no mixing of sediment. We modeled the expected ^{10}Be concentration at depth (see section 3.2) for a range of exposure times (t = 0 – 500 ka; 200 a resolution), terrace erosion rates (ε = 0 – 3 mm ka^{-1}; 0.01 mm ka^{-1} resolution) and inherited ^{10}Be concentrations (0 – 180,000 atoms g^{-1}; 30000 atoms g^{-1}

resolution) to obtain the parameters that yielded the minimum value for the sum of chi-squared ($\Sigma\chi^2_{min}$). The terrace erosion rate was restricted to positive values in this exercise because pedologic evidence (Section 3.1.1) and geomorphic observations indicate deflation (as opposed to inflation) of the terrace surface (Section 3.1.2). The best fit ($\Sigma\chi^2_{min}$) occurs with 233.8 ka exposure, a terrace erosion rate of 0 mm ka^{-1} and no inherited nuclides (Figure 6). Figure 6a is the $\log_{10}\Sigma\chi^2$ solution surface for the case of no inheritance. The 1σ and 2σ analytical uncertainty contours illustrate the strong correlation between the uncertainties in exposure age and erosion rate. The contours include a wide range of potential exposure age/erosion rate solutions.

The reduced chi-squared χ^2_r value of 0.97 indicates the model fit is as good as can be expected given the measurement uncertainties. Figure 7a provides the predicted concentrations, based on the parameters obtained from the best-fit exposure model, against the measured data points. The deepest sample is critical to defining the best-fit parameters. Several exposure age/erosion rate solutions can fit the near surface data well, but are less able to fit the deepest sample. Figure 7b gives the predicted nuclide concentration for two exposure age/erosion rate scenarios that fit most measured data points well, except the deepest samples. This illustrates the importance of deep samples to obtain robust age constraints from depth, and the value of forward modeling to obtain the best fitting parameters.

4.2.3 Outwash cobbles

Cobbles from the associated outwash terrace yield ^{10}Be exposure ages that are consistently older than boulder ages, ranging from 193.6 – 265.1 ka. Exposure ages

from sample sites S1 and S2 are indistinguishable (Table 2, Figures 4-5). The high variability in exposure ages likely stems from geomorphic processes as opposed to variable inherited nuclides. While the depth profile indicates that the terrace sediment has remained stable below 10 cm, all surface cobbles have similar or higher nuclide concentrations than the concentration at 10 cm in the profile. Thus a combination of near surface turbation (e.g., cryoturbation) above 10 cm and terrace erosion by deflation can explain the observed age range. The geologic evidence supports deflation of the terrace surface (Section 3.1.2), causing previously buried cobbles to become exposed in the process (Figure 7c). The scenario is consistent with an observation that the youngest samples at S2 fully retained their fluvial shape, while the oldest cobbles revealed significant ventifaction (Figure 3f, 3g). With no lithologic difference between cobbles, we infer that ventifaction of surface cobbles indicates a longer surface residence time. The two oldest surface cobbles yield an arithmetic mean age of 260.6 ± 6.5 ka (1σ external ± 34 ka; Figure 5). The old ages are unlikely to be the result of re-working of older sediment based on our assessment of nuclide inheritance (Section 5.1) and also because alluvial fans composed of older (Caracoles) sediment are clearly defined and over 5 km from the sampled location (Figure 4). The $^{26}Al/^{10}Be$ ratios are consistent with a relatively simple exposure history without prolonged burial.

5. DISCUSSION

5.1 Nuclide inheritance

We assess nuclide inheritance based on the ^{10}Be concentration depth-profile of pebble clasts, which averages inheritance over 10 to 50 individual pebble clasts per sample at each of the eight sample depths. These data indicate that the average inherited nuclide component in the Hatcher outwash terrace is negligible (Figure 6b). This is in agreement with the low variability of ages found in outwash cobbles from the younger Río Blanco unit (σ = 0.5 ka), which suggests that the variability of inherited nuclides is low (i.e., within analytical uncertainties), and by inference inheritance (if inheritance would be large, its variability would be large). Thus we conclude that nuclide inheritance is negligible in outwash deposits of the Río Blanco and Hatcher units, and probably throughout the Lago Pueyrredón valley.

5.2 Age of the Hatcher Unit

The Hatcher moraines and associated outwash terraces were deposited roughly coincidently, yet exposure ages differ by over 200 ka depending on the sample and nature of the sample location. Because nuclide inheritance is demonstrably low and most geologic processes act to reduce cosmogenic nuclide inventories (Phillips et al., 1990), the oldest ages are considered the best estimate for the deposition age of the unit. The oldest surface cobbles are likely closest to the deposition age at 260.6 ± 6.5 ka, analogous to the oldest boulder ages on a moraine (cf. Zreda and Phillips, 1995). This age is ~25 ka older than that indicated by the depth-profile $\Sigma\chi^2_{min}$ best-fit at 233.8 ka, but is indistinguishable at 1σ (Figure 6a). The statistical best-fit ($\Sigma\chi^2_{min}$) occurs with a terrace erosion rate of 0 mm ka^{-1}. The geologic evidence, however, suggests minor terrace deflation (Section 3.1.2). Changes in bulk density occurring temporally (e.g., with soil and pedogenic carbonate formation) may have influenced the $\Sigma\chi^2_{min}$ fit,

but the effect cannot be accurately accounted for and is expected to be small relative to age uncertainty. A terrace age of 260.6 ka corresponds with an inferred terrace erosion rate of ca. 0.53 mm ka^{-1} based on the depth-profile (χ_r^2= 1.12; Figures 6a,7c). This suggests ~14 cm of terrace deflation over the exposure duration, with survival of the oldest clasts likely due to their resistant lithology. This amount of surface lowering is consistent with minor terrace deflation inferred at the sampled sites and with preservation of shallow surface channels with clear braiding patterns (~50cm relief). The $^{26}Al/^{10}Be$ ratios of surface cobbles and the depth-profile data are consistent with a single stage exposure history. Based on current knowledge of ^{10}Be production rates and the assumptions made in this paper, we estimate the age of the Hatcher unit to be 260.6 ± 6.5 ka (1σ external ± 34 ka; ε_{terr} = 0.53 mm ka^{-1}).

Of the five scaling schemes implemented in the CRONUS-Earth exposure age calculator, the time-dependent Lal (1991)/Stone (2000) scaling factors yield the youngest exposure ages by ~5%. Using these scaling factors reduces the interpreted minimum age to 248 ± 24 ka (1σ external). Within uncertainty this overlaps with the age of substage 7d (~ 225 - 220 ka, Martinson et al., 1987). However, substage 7d is short-lived relative to both MIS 6 and 8. The Hatcher unit is older than MIS 6, and its size and preservation suggests it was more extensive than MIS 6. Thus we consider it unlikely that the Hatcher moraines are age-equivalent to the short-lived 7d substage, and consider it more likely that they are coeval with the more pronounced global cooling during MIS 8, as indicated by our estimated exposure age.

5.2.1 Discordant ages

The above results indicate that in certain environments the outwash terrace is a better target for exposure dating old glacial events than the associated moraine. Outwash samples yield consistently older exposure ages than those from the moraines (Figure 5). This result was expected based on the favorable environmental conditions and local geomorphology (Section 1.3 – 2). However, the significant disparity in ages between moraine boulders and outwash cobbles was not predicted. While large scatter is expected of old moraine boulders, the oldest age was thought to date closely moraine deposition. In this case, that age was more than 100 ka too young. Putkonen and Swanson (2003) recommend sampling at least 6 – 7 boulders from old and tall moraines to obtain a boulder age at ≥ 90% of the moraine age (95% confidence). Therefore we cannot rule-out under-sampling as a cause of the discrepancy. However, well-preserved boulders were rare.

The $^{26}Al/^{10}Be$ ratios provide no evidence to explain the young boulder ages. Boulder erosion rate uncertainty could explain the wide scatter and young ages, but the moraine cobble data (where negligible erosion is implicit) indicate that exhumation (moraine degradation) is likely the primary control. The moraine cobble with the highest ^{10}Be concentration (5.26×10^5 atoms g^{-1}) is used to infer minimum moraine degradation rates using model scenarios (Equation 1) that assume a deposition age of 260 ka and a till density of 2.2 g cm^{-3}. The minimum amount occurs with instant degradation of ~101 cm at the time of sampling. By comparison, the concentration can be achieved with a constant degradation rate of 12 mm ka^{-1}, equating to ~3.1 meters of surface lowering. The tallest boulder (2.0 m) has an exposure age within 30% of the age of the outwash terrace, which may indicate a relatively small amount

of original cover. Concluding, we infer that boulder exhumation is the primary cause of the young and scattering boulder exposure ages.

However, additional complexity may have been introduced by episodic boulder erosion. If significant aeolian erosion occurs when outwash plains are active (Section 2.2), then aeolian erosion episodes probably occurred during MIS 6 (ca. 150 ka) and during deposition of the Río Blanco outwash at ~25 ka. Because the erosion rate applied is a long-term average, a relatively recent pulse of boulder erosion may yield exposure ages that are too young (e.g., Small et al., 1997). However, aeolian erosion is normally restricted to less than 50 cm above the soil surface (Bagnold, 1941), thus the taller boulders may not have experienced it in the geologically recent past.

Moraine cobbles are rarely ventifacted, suggesting exhumation occurred after any recent (aeolian) erosion episode. For the sake of argument, if we assume soil degradation at a constant rate, the derived rate (12 mm ka^{-1}) is nearly double the maximum rate estimated for the older and more subdued Telken moraines at LBA (ca. 7 mm ka^{-1}; Ackert and Mukhopadhyay, 2005). By comparison, the Hatcher moraines are relatively sharp crested at the sampled locations (Figure 3c,d). Because environmental conditions are similar, the different rates could be explained by a differing moraine surface morphology. Models predict higher degradation on tall and steeply dipping moraines (Putkonen and O'Neal, 2006; Putkonen and Swanson, 2003). At the sampled location, the ice-contact flank of the moraine was taller (40 – 50 m high) and steeper dipping (19º – 25º) than both the down-ice flank, and more subdued terminal locations. It is possible this 'lateral moraine' morphology at the sampled locations could result in locally high degradation. If so, the large discrepancy in

boulder and outwash ages could be due in part to our choice of sample location, despite seemingly good preservation.

Regardless of the cause, our data highlight the significant challenges of exposure dating old glacial deposits using moraine boulders. Despite probable exhumation of all boulder samples and complexity introduced by boulder erosion, the data yield a typical spread of ages with the oldest boulder age (no erosion) and the average age (w/erosion) indistinguishable. This together with an observation of moraine ridges as old as 1.1 Ma still clearly preserved (Figure 2) would suggest that moraine degradation rates are generally low in this environment. Given only this information, it would be reasonable to assume the exposure ages from boulder samples (~150 ka) dated closely moraine deposition. However, this interpretation would be erroneous by over 100 ka. It is worth noting that small moraine cobbles are highly sensitive to moraine degradation in this environment, these samples yield exposure ages that underestimate the deposition age by over 200 ka. These results highlight the challenge of exposure dating old moraines and suggest a cautious approach to interpreting such data.

5.3 Correlation to LBA record

The new cosmogenic exposure ages allow comparison to the record at LBA. We re-calculate the ^{10}Be boulder exposure ages published by Kaplan et al. (2004; 2005) and Douglass et al. (2006) for both the Fenix V and Moreno II moraines in order to compare directly the data presented in this study and the assumptions therein. The Río Blanco – Fenix correlation is valid based on LGM ages of 26.8 ± 1.0 ka and 24.5

± 1.3 ka for the Río Blanco and Fenix moraines, respectively. The Hatcher – Moreno correlation is less convincing. On Moreno II, the oldest ^{10}Be boulder exposure age (no erosion) of 169.4 ka and mean age (w/erosion) of 168.8 ka is indistinguishable from the Hatcher boulders. If the supposed correlation is valid, then the Moreno moraines were also deposited at ~260 ka, and the young boulder exposure ages on the Moreno moraines are analogous to those of the Hatcher moraines. Alternatively, the correlation may not be valid and these are indeed two different glacial events preserved separately in each valley.

The available evidence supports the latter interpretation. First, the lowest ^{10}Be concentration of 5 moraine cobbles on Moreno I was found to be ~7.30 x 10^5 atoms g^{-1} (Table 3). With steady degradation, this concentration can be achieved with rates of 6.1 and 7.6 mm ka^{-1} for a surface ~170 ka (oldest boulder age) and ~260 ka (Hatcher age), respectively. These rates are consistent with the maximum rate estimated for the Telken moraines in this valley (Ackert and Mukhopadhyay, 2005), and equate to roughly 105 – 200 cm of moraine surface lowering. Thus degradation rates are apparently lower for the Moreno moraines and boulders may have been continuously exposed. Second, 6-7 boulders (cf. Putkonen and Swanson, 2003) between 5 – 200 cm height were measured from the Moreno I-II moraines; these were age consistent (Kaplan et al., 2005). Third, ^{230}Th/U dating of soil carbonate formed in outwash gravels associated with the Moreno II moraines suggest onset of calcic pedogenesis at 170 ± 8.3 ka (Phillips et al., 2006). ^{230}Th/U data from the younger Fenix moraines indicates a brief interval (< 3 ka) between surface stabilization and the onset of calcic pedogenesis under glacial conditions. The re-calculated ^{10}Be boulder exposure ages are consistent with this new data. Therefore, based on the available evidence, the best

estimate for the age of the Moreno I-II moraines is before ~170 ka, or MIS 6, and thus the correlation to the Hatcher moraines appears invalid on this basis.

6. CONCLUSIONS

- We demonstrate that outwash terrace sediments are better targets than associated moraine boulders for exposure dating 'old' (i.e., pre-LGM) glacial deposits in the Lago Pueyrredón valley, central Patagonia. A comparatively small number of outwash samples provide more consistently accurate results.
- We find that exposure ages from moraine boulders underestimate the deposition age by ~100 ka, and exposure ages from moraine cobbles underestimate the deposition age by over 200 ka. We infer that exhumation as a consequence of moraine degradation is the primary cause of the age discrepancy between the moraine and outwash samples.
- A forward model inversion of a ^{10}Be depth-profile in the outwash terrace sediment, using the sum of chi-squared, is used to define the exposure age, erosion rate and inherited ^{10}Be concentration. This model, in conjunction with geologic observations and exposure ages from surface cobbles, indicates a terrace age of ca. 260 ka, a low terrace erosion rate of ca. 0.5 mm ka^{-1}, and no inherited nuclides.
- The result indicates that a major advance of a Patagonian ice sheet occurred at ~260 ka (MIS 8) and deposited the Hatcher moraines at Lago Pueyrredón. This finding differs from findings at Lago Buenos Aires, where the Moreno I-II moraines, which occupy a similar stratigraphic position relative to the LGM

deposits, are dated to MIS 6 (Kaplan et al., 2005). This documents the value of more than one site in a region for reconstructing glacial chronologies.

- The local LGM maximum occurred at ~27 – 25 ka and is represented by the Río Blanco moraine system.
- No deposits relating to MIS 6 or MIS 4 were observed at Lago Pueyrredón.
- Our ages for the Río Blanco and Hatcher moraines are discrepant with the previously inferred chronology (Wenzens, 2005).

ACKNOWLEDGEMENTS

We thank C. Risso, P. Alvarez and O. Martínez for logistical support; A-S. Meriaux for fieldwork support; S. Binnie and E. McDougall for assistance with laboratory work and D. Sugden for helpful comments. We thank the UK Natural Environment Research Council, the Royal Geographic Society (with IBG) - Rio Tinto plc award, the Royal Scottish Geographic Society and the Carnegie Trust for the Universities of Scotland for support of this study. We thank the Scottish Universities Environmental Research Centre (S.U.E.R.C.) for sample analysis. We are grateful for the constructive comments of two anonymous reviewers that greatly improved the manuscript. This is L-DEO contribution number #XXXX.

Figure 1

a) Location of study area showing an expanded Patagonian ice sheet and the present day North (NPI) and South (SPI) Patagonian Icefields with

glacial/interglacial specific drainage pattern. The Rio Baker presently drains both Lago Buenos Aires (LBA) and Lago Pueyrredón (LP).

b) The over-deepened (white=high elevation) LBA and LP outlet valleys with comparison of the broad glacial stratigraphy and mapping of Caldenius (1932). The chronology at LBA is based on cosmogenic exposure ages (^{3}He, ^{10}Be, ^{26}Al) by Kaplan et al. (2004, 2005) and Douglass et al. (2006) and limiting ^{40}Ar/^{39}Ar ages by Singer et al. (2004). The naming convention used for glacial units in the LP valley is based on Caldenius (1932).

Figure 2

DEM (SRTM 90m, artificially illuminated) of the LP valley showing ice limits of the four major glacial units and the exceptional preservation of moraine and outwash terraces. The well-preserved moraines of the Gorra de Poivre ice limit are inferred to be 1.1 Ma. The sampled locations for each sample type in this study are shown along with ^{14}C dates by Wenzens (2005) and Mercer (1982) and magnetic polarity measurements by Sylwan et al. (1991)(see section 2.3).

Figure 3

a) Granite moraine boulder with flutings demonstrating the erosive power of debris laden wind. Varying degrees of wind erosion is common to moraine boulders and outwash cobbles.

b) Quartz pebble from the Hatcher outwash terrace (S1) showing rock varnish on ventifacts which suggests aeolian erosion is episodic.

c) The tallest (2m) and oldest boulder sampled from the sharp-crested Hatcher moraine on the north side of valley.

d) The Hatcher moraine crest on the south side of the valley, showing a desert pavement of cobble and pebble clasts.

e) Photo of the depth-profile location with pedogenic carbonate formation below ~30cm depth. The top of the profile was undisturbed and vegetated. The top 10 cm of the profile contains less than ~30% fine material.

f) The youngest surface cobbles at S2 retained their fluvial shape, indicating relatively recent exhumation.

g) The oldest surface cobbles at S2 showed significant wind erosion (ventifacted facet at the top right of the cobble) indicating a long surface residence time.

Figure 4

Geomorphic map of the Hatcher moraines and outwash terraces on the north side of valley (location shown in Figure 2), showing sample locations and exposure ages. Three small (1 – 3m difference in elevation) terrace levels related to recessional moraine limits are clearly distinguished close to their associated moraines, but grade to a common base level further east. Outwash was sampled at two sites (S1 and S2). S1 can be directly mapped to the dated moraine while S2 is located 8 km NE at a point where the small terrace levels coalesce; the exposure ages obtained from

samples from S1 and S2 are indistinguishable. The location of outwash fans composed of older "Caracoles" material is shown. DP: depth-profile location.

Figure 5

^{10}Be exposure ages obtained from samples of the Río Blanco and Hatcher units at Lago Pueyrredón, 47.5º S, Argentina, compared to the Vostok temperature curve (Petit et al., 1999). Data is ordered by sample type. Cartoon depicts moraine and outwash positions but is not to scale. S1 and S2 refer to sample sites on Hatcher outwash terrace (Figure 4). Exposure ages obtained using the CRONUS-Earth exposure age calculator (http://hess.ess.washington.edu/math/index.html) version 2.2 (Balco et al., 2008) with a 5% higher production rate for Hatcher samples (Section 3.3) and Dunai (2001) scaling factors. Uncertainties are 1σ analytical. Boulder erosion rates from Kaplan et al. (2005). The Río Blanco data show little variability compared to the Hatcher data. The mean of the two oldest outwash terrace cobbles (red-line) is the interpreted age of the glacial advance, moraine boulders under-estimate this age by ~ 100 ka. See Table 2 for full sample details.

Figure 6

a) Plot of the gridded $\log_{10}(\Sigma\chi^2)$ values for a range of exposure ages and erosion rates for the case of no inherited nuclides; the plot is based on the depth-profile data and exposure model optimization. The sensitivity to inheritance is illustrated in Figure 6b. The best-fit (star) occurs with an exposure age of 233.8 ka, an erosion rate of 0 mm ka^{-1} and no inherited

nuclides. Contours are increments of 0.5 from the $\log_{10}(\Sigma\chi^2)$ minimum. The uncertainty contours mark the probability of occurrence (0.68/1σ, 0.90/2σ) for 5 degrees of freedom. The model fits analytical sources of uncertainty as discussed in the text. The uncertainties of exposure age and erosion rate are strongly correlated. The inferred terrace age, based on the mean exposure age of the oldest surface cobbles (these were not included in the profile optimization), corresponds to a terrace erosion rate of ~0.53 mm ka^{-1}.

b) Plot showing the effect of varying the exposure age, erosion rate and ^{10}Be inheritance on the $\Sigma\chi^2$ minimum value for a range of inheritance values. The maximum inheritance value was obtained from the nuclide concentration of the deepest sample in the profile (Table 1). The $\Sigma\chi^2_{min}$ steadily increases as the total inheritance increases; thus the best fit occurs with no inherited nuclides.

Figure 7

Measured ^{10}Be concentration as a function of depth within the Hatcher outwash terrace. Data points (solid circles) are an amalgamation of pebble clasts following Repka et al. (1997) (Table 1). The (1σ) analytical uncertainties in ^{10}Be concentration were used in the model optimization. The uncertainty with depth is based on the thickness of the largest clast (Table 1).

a) Plot of modeled best-fit ($\Sigma\chi^2_{min}$) ^{10}Be concentration based on the exposure model optimization.

b) Plot of a scenario where the near surface data are well approximated while the deepest samples are not. This exemplifies the importance of deep profiles with several data points, and the value of exposure model optimization. The parameters of exposure age and erosion rate were obtained from the $\Sigma\chi^2$ solution surface (Figure 6a).

c) Plot of the modeled ^{10}Be concentration based on the exposure age of the oldest surface cobbles, and the corresponding erosion rate inferred from the $\Sigma\chi^2$ solution surface (Figure 6a). The cartoon illustrates how a combination of terrace deflation and shallow turbation (< 10cm) can explain the wide range of measured ^{10}Be concentrations in surface cobbles.

REFERENCES CITED

Ackert, R. P., and Mukhopadhyay, S. (2005). Constraining landform erosion and ages from surface exposure age distributions on old Patagonian moraines. *Geochimica et Cosmochimica Acta* **69,** A162.

Ackert, R. P., Singer, B. S., Guillou, H., Kaplan, M. R., and Kurz, M. D. (2003). Long-term cosmogenic He-3 production rates from Ar-40/Ar-39 and K-Ar dated Patagonian lava flows at 47 degrees S. *Earth and Planetary Science Letters* **210,** 119-136.

Anderson, R. S., Repka, J. L., and Dick, G. S. (1996). Explicit treatment of inheritance in dating depositional surfaces using in situ Be-10 and Al-26. *Geology* **24,** 47-51.

Bagnold, R. A. (1941). "The Physics of Blown Sand and Desert Dunes." Chapman Hall, London.

Balco, G., Stone, J. O., Lifton, N. A., and Dunai, T. J. (2008). A complete and easily accessible means of calculating surface exposure ages or erosion rates from Be-10 and Al-26 measurements. *Quaternary Geochronology* **3,** 174-195.

Benson, L., Madole, R., Phillips, W., Landis, G., Thomas, T., and Kubik, P. (2004). The probable importance of snow and sediment shielding on cosmogenic ages of north-central Colorado Pinedale and pre-Pinedale moraines. *Quaternary Science Reviews* **23,** 193-206.

Bevington, P., and Robinson, K. (2003). "Data Reduction and Error Analysis for the Physical Sciences." McGraw-Hill.

Briner, J. P., Kaufman, D. S., Manley, W. E., Finkel, R. C., and Caffee, M. W. (2005). Cosmogenic exposure dating of late Pleistocene moraine stabilization in Alaska. *Geological Society Of America Bulletin* **117,** 1108-1120.

Brocard, G. Y., van der Beek, P. A., Bourles, D. L., Siame, L. L., and Mugnier, J. L. (2003). Long-term fluvial incision rates and postglacial river relaxation time in

the French Western Alps from Be-10 dating of alluvial terraces with assessment of inheritance, soil development and wind ablation effects. *Earth and Planetary Science Letters* **209,** 197-214.

Caldenius, C. R. C. (1932). "Las glaciaciones cuaternarias en la Patagonia y Tierra del Fuego : una investigación regional, estratigráfica y geocronológica : una comparación con la escala geocronológica sueca : with an English summary." [Stockholms högskola], Stockholm.

Chadwick, O. A., Hall, R. D., and Phillips, F. M. (1997). Chronology of Pleistocene glacial advances in the central Rocky Mountains. *Geological Society of America Bulletin* **109,** 1443-1452.

Chorley, R. J., Schumm, S. A., and Sugden, D. E. (1984). "Geomorphology." Methuen, London, New-York.

Clapperton, C. M. (1993). "Quaternary Geology and Geomorphology of South America." Elsevier Science Publishers B. V., Amsterdam.

Douglass, D. C., Singer, B. S., Kaplan, M. R., Mickelson, D. M., and Caffee, M. W. (2006). Cosmogenic nuclide surface exposure dating of boulders on last-glacial and late-glacial moraines, Lago Buenos Aires, Argentina: Interpretive strategies and paleoclimate implications. *Quaternary Geochronology* **1,** 43-58.

Dunai, T. J. (2001). Influence of secular variation of the geomagnetic field on production rates of in situ produced cosmogenic nuclides. *Earth and Planetary Science Letters* **193,** 197-212.

Flint, R. F., and Fidalgo, F. (1964). Glacial Geology Of The East Flank Of The Argentine Andes Between Latitude 39-Degrees-10's And Latitude 41-Degrees-20's. *Geological Society of America Bulletin* **75,** 335.

Gillespie, A. R., and Bierman, P. R. (1995). Precision of terrestrial exposure ages and erosion rates estimated from analysis of cosmogenic isotopes produced in situ. *Journal of Geophysical Research-Solid Earth* **100,** 24637-24649.

Gosse, J. C., and Phillips, F. M. (2001). Terrestrial in situ cosmogenic nuclides: theory and application. *Quaternary Science Reviews* **20,** 1475-1560.

Granger, D. E., and Smith, A. L. (2000). Dating buried sediments using radioactive decay and muogenic production of Al-26 and Be-10. *Nuclear Instruments & Methods in Physics Research Section B-Beam Interactions with Materials and Atoms* **172,** 822-826.

Hallet, B., and Putkonen, J. (1994). Surface Dating Of Dynamic Landforms - Young Boulders On Aging Moraines. *Science* **265,** 937-940.

Hancock, G. S., Anderson, R. S., Chadwick, O. A., and Finkel, R. C. (1999). Dating fluvial terraces with Be-10 and Al-26 profiles: application to the Wind River, Wyoming. *Geomorphology* **27,** 41-60.

Hulton, N. R. J., Purves, R. S., McCulloch, R. D., Sugden, D. E., and Bentley, M. J. (2002). The Last Glacial Maximum and deglaciation in southern South America. *Quaternary Science Reviews* **21,** 233-241.

Inbar, M., Ostera, H. A., Parica, C. A., Remesal, M. B., and Salani, F. M. (1995). Environmental Assessment of 1991 Hudson Volcano Eruption Ashfall Effects on Southern Patagonia Region, Argentina. *Environmental Geology* **25,** 119-125.

Kaplan, M. R., Ackert, R. P., Singer, B. S., Douglass, D. C., and Kurz, M. D. (2004). Cosmogenic nuclide chronology of millennial-scale glacial advances during O-isotope stage 2 in Patagonia. *Geological Society of America Bulletin* **116,** 308-321.

Kaplan, M. R., Coronato, A., Hulton, N. R. J., Rabassa, J. O., Kubik, P. W., and Freeman, S. (2007). Cosmogenic nuclide measurements in southernmost South America and implications for landscape change. *Geomorphology* **87,** 284-301.

Kaplan, M. R., Douglass, D. C., Singer, B. S., and Caffee, M. W. (2005). Cosmogenic nuclide chronology of pre-last glacial maximum moraines at Lago Buenos Aires, 46 degrees S, Argentina. *Quaternary Research* **63,** 301-315.

Kaplan, M. R., Hein, A. S., Hubbard, A., and Lax, S. M. (2009). Can glacial erosion limit the extent of glaciation? *Geomorphology* **103,** 172-179.

Kaplan, M. R., Singer, B. S., Douglass, D. C., Ackert, R. P., and Caffee, M. W. (2006). Comment on: Cosmogenic nuclide chronology of pre-last glacial maximum moraines at Lago Buenos Aires, 46 degrees S, Argentina (Quaternary Research 63/3, 2005, 301-315) - Reply. *Quaternary Research* **66,** 367-369.

Lal, D. (1991). Cosmic-Ray Labeling Of Erosion Surfaces - Insitu Nuclide Production-Rates And Erosion Models. *Earth And Planetary Science Letters* **104,** 424-439.

Martinson, D. G., Pisias, N. G., Hays, J. D., Imbrie, J., Moore, T. C., and Shackleton, N. J. (1987). Age Dating and the Orbital Theory of the Ice Ages - Development of a High-Resolution-0 to 300,000-Year Chronostratigraphy. *Quaternary Research* **27,** 1-29.

Meglioli, A. (1992). "Glacial geology and chronology of southernmost Patagonia and Tierra del Fuego, Argentina and Chile." Lehigh University.

Mercer, J. H. (1976). Glacial History Of Southernmost South-America. *Quaternary Research* **6,** 125-166.

Mercer, J. H. (1982). Holocene glacier variations in southern South America. *Striae* **18,** 35-40.

Nishiizumi, K. (2004). Preparation of Al-26 AMS standards. *Nuclear Instruments & Methods in Physics Research Section B* **223-24,** 388-392.

Nishiizumi, K., Imamura, M., Caffee, M. W., Southon, J. R., Finkel, R. C., and McAninch, J. (2007). Absolute calibration of Be-10 AMS standards. *Nuclear Instruments & Methods in Physics Research Section B* **258,** 403-413.

Owen, L. A., Caffee, M. W., Bovard, K. R., Finkel, R. C., and Sharma, M. C. (2006). Terrestrial cosmogenic nuclide surface exposure dating of the oldest glacial successions in the Himalayan orogen: Ladakh Range, northern India. *Geological Society Of America Bulletin* **118,** 383-392.

Petit, J. R., Jouzel, J., Raynaud, D., Barkov, N. I., Barnola, J. M., Basile, I., Bender, M., Chappellaz, J., Davis, M., Delaygue, G., Delmotte, M., Kotlyakov, V. M., Legrand, M., Lipenkov, V. Y., Lorius, C., Pepin, L., Ritz, C., Saltzman, E., and Stievenard, M. (1999). Climate and atmospheric history of the past 420,000 years from the Vostok ice core, Antarctica. *Nature* **399,** 429-436.

Phillips, F. M., Zreda, M. G., Evenson, E. B., Hall, R. D., Chadwick, O. A., and Sharma, P. (1997). Cosmogenic Cl-36 and Be-10 ages of Quaternary glacial and fluvial deposits of the Wind River Range, Wyoming. *Geological Society of America Bulletin* **109,** 1453-1463.

Phillips, F. M., Zreda, M. G., Smith, S. S., Elmore, D., Kubik, P. W., and Sharma, P. (1990). Cosmogenic Chlorine-36 Chronology for Glacial Deposits at Bloody Canyon, Eastern Sierra-Nevada. *Science* **248,** 1529-1532.

Phillips, R. J., Sharp, W. D., Singer, B. S., and Douglass, D. C. (2006). Utilising U-series disequilibria of calcic soils to constrain the surface age of Quaternary

deposits: A comparison with 10Be, 26 Al age data from Patagonian glacial moraines. *Geochimica et Cosmochimica Acta* **70,** A491.
Putkonen, J., Connolly, J., and Orloff, T. (2008). Landscape evolution degrades the geologic signature of past glaciations. *Geomorphology* **97,** 208-217.
Putkonen, J., and O'Neal, M. (2006). Degradation of unconsolidated Quaternary landforms in the western North America. *Geomorphology* **75,** 408-419.
Putkonen, J., and Swanson, T. (2003). Accuracy of cosmogenic ages for moraines. *Quaternary Research* **59,** 255-261.
Rabassa, J., and Clapperton, C. M. (1990). Quaternary Glaciations Of The Southern Andes. *Quaternary Science Reviews* **9,** 153-174.
Rabassa, J., Coronato, A., Bujalesky, G., Salemme, M., Roig, C., Meglioli, A., Heusser, C., Gordillo, S., Roig, F., Borromei, A., and Quattrocchio, M. (2000). Quaternary of Tierra del Fuego, Southernmost South America: an updated review. *Quaternary International* **68,** 217-240.
Repka, J. L., Anderson, R. S., and Finkel, R. C. (1997). Cosmogenic dating of fluvial terraces, Fremont River, Utah. *Earth and Planetary Science Letters* **152,** 59-73.
Schäfer, J. M., Oberholzer, P., Zhao, Z., Ivy-Ochs, S., Wieler, R., Baur, H., Kubik, P. W., and Schluchter, C. (2008). Cosmogenic beryllium-10 and neon-21 dating of late Pleistocene glaciations in Nyalam, monsoonal Himalayas. *Quaternary Science Reviews* **27,** 295-311.
Schildgen, T., Dethier, D. P., Bierman, P., and Caffee, M. (2002). Al-26 and Be-10 dating of late Pleistocene and Holocene fill terraces: A record of fluvial deposition and incision, Colorado Front Range. *Earth Surface Processes and Landforms* **27,** 773-787.
Shanahan, T. M., and Zreda, M. (2000). Chronology of quaternary glaciations in East Africa. *Earth and Planetary Science Letters* **177,** 23-42.
Singer, B. S., Ackert, R. P., and Guillou, H. (2004). Ar-40/Ar-19 and K-Ar chronology of Pleistocene glaciations in Patagonia. *Geological Society of America Bulletin* **116,** 434-450.
Singer, B. S., and Pringle, M. S. (1996). Age and duration of the Matuyama-Brunhes geomagnetic polarity reversal from Ar-40/Ar-39 incremental heating analyses of lavas. *Earth and Planetary Science Letters* **139,** 47-61.
Small, E. E., Anderson, R. S., Repka, J. L., and Finkel, R. (1997). Erosion rates of alpine bedrock summit surfaces deduced from in situ Be-10 and Al-26. *Earth and Planetary Science Letters* **150,** 413-425.
Staiger, J., Gosse, J., Toracinta, R., Oglesby, B., Fastook, J., and Johnson, J. V. (2007). Atmospheric scaling of cosmogenic nuclide production: Climate effect. *Journal of Geophysical Research-Solid Earth* **112**.
Stone, J. O. (2000). Air pressure and cosmogenic isotope production. *Journal Of Geophysical Research-Solid Earth* **105,** 23753-23759.
Suárez, M., and De La Cruz, R. (2001). Jurassic to miocene K-Ar dates from eastern central Patagonian Cordillera plutons, Chile (45 degrees-48 degrees S). *Geological Magazine* **138,** 53-66.
Sugden, D. E., McCulloch, R. D., Bory, A., and Hein, A. S. (2009). Influence of Patagonian glaciers on Antarctic dust deposition during the last glacial period. *Nature Geoscience* **d.o.i. (10.1038/NGEO474)**.
Sylwan, C., Beraza, L., and Caselli, A. (1991). Magnetoestratigrafia de la secuencia morenica en el valle del Lago Pueyrredon, provincia de Santa Cruz. *Asociacion Geologica Argentina, Rev.* **XLVI,** 235-238.

Ton-That, T., Singer, B., Mörner, N., and Rabassa, J. (1999). Datación de lavas basalticas por 40Ar/39Ar geología glacial de la region del lago Buenos Aires, provincia de Santa Cruz, Argentina. *Revisita de la Asociación Geológica Argentina* **54,** 333-352.

Vermeesch, P. (2007). CosmoCalc: An Excel add-in for cosmogenic nuclide calculations. *Geochemistry Geophysics Geosystems* **8**.

Wenzens, G. (2005). Glacier advances east of the Southern Andes between the Last Glacial Maximum and 5,000 BP compared with lake terraces of the endorrheic Lago Cardiel (49 degrees S, Patagonia, Argentina). *Zeitschrift Für Geomorphologie* **49,** 433-454.

Wenzens, G. (2006). Comment on: Cosmogenic nuclide chronology of pre-last glacial maximum moraines at Lago Buenos Aires, 46 degrees S, Argentina (Quaternary Research 63/3, 2005, 301-315). *Quaternary Research* **66,** 364-366.

Zentmire, K. N., Gosse, J., Baker, C., McDonald, E., and Wells, S. (1999). The problem of inheritance when dating alluvial fans and terraces with TCN: Insight from the Matanuska Glacier. *GSA Abstracts and Programs* **31**.

Zreda, M. G., and Phillips, F. M. (1995). Insights into alpine moraine development from cosmogenic Cl-36 buildup dating. *Geomorphology* **14,** 149-156.

Zreda, M. G., Phillips, F. M., and Elmore, D. (1994). Cosmogenic Cl-36 Accumulation in Unstable Landforms .2. Simulations and Measurements on Eroding Moraines. *Water Resources Research* **30,** 3127-3136.

Supplementary material for on-line publication only

Click here to download Supplementary material for on-line publication only: Hein_supplement.doc

Table 1

Click here to download Table: Hein_Table1.doc

Table 1: ^{10}Be data for depth-profile in Hatcher outwash terrace.

Sample ID – AMS ID	Latitude (dd)	Longitude (dd)	Altitude (m asl)	Depth (cm)	# clasts	Thickness[a] (cm)	Quartz mass (g)	^{10}Be measured[b] (10^6 atom g^{-1}) (±1σ)
depth-profile (S2)								
BC07-48a – b2068	-47.26627	-70.96320	583	10	41	3	21.65	1.508 ± 0.047
BC07-48b – b2067				20	14	3.5	27.42	1.242 ± 0.039
BC07-48c – b2066				30	10	3.5	39.06	1.153 ± 0.033
BC07-48d – b2063				40	18	4	46.18	0.948 ± 0.029
BC07-48e – b2062				50	37	4	58.19	0.802 ± 0.023
BC07-48f – b2061				75	19	4	63.82	0.563 ± 0.018
BC07-48g – b2048				100	49	3.5	59.44	0.381 ± 0.010
BC07-48h – b2060				150	44	3	61.54	0.184 ± 0.006

a. Thickness of largest clast included in profile; this is used as a measure of depth uncertainty in the profile. b. Nuclide concentrations are normalized to revised ^{10}Be standards and half-life (1.36 Ma) of Nishiizumi et al. (2007) and include propagated AMS sample/lab-blank uncertainty and 2% carrier mass uncertainty. Clast density 2.7 g cm^{-3}. Topographic shielding at the profile site is negligible. All AMS measurements made at S.U.E.R.C.

Table 2

Click here to download Table: Hein_Table2.doc

Table 2: ^{10}Be and ^{26}Al data for Río Blanco and Hatcher moraines and outwash terraces.

Sample I.D.		Latitude	Longitude	Altitude	Boulder height	Thickness	Quartz mass	Isotope - AMS ID[a]	Nuclide concentration[a]	^{26}Al/^{10}Be[b]	Age 1[c,d] (10^3 yrs) ε = 0		Age 2[c,d,e] (10^3 yrs) ε = 1.4 mm ka^{-1}	
		(dd)	(dd)	(m asl)	(cm)	(cm)	(g)		(10^6 atom g^{-1})		Age + 1σ (int)	± 1σ (ext)	Age + 1σ (int)	± 1σ (ext)
Río Blanco[d]														
moraine boulder														
BC07-7		-47.5186	-71.2361	564	225	2.5	20.9284	^{10}Be – b2050	0.200 ± 0.007	-	27.1 ± 0.9	3.3	28.0 ± 0.9	3.6
BC07-8		-47.5564	-71.2629	587	190	1.5	27.7948	^{10}Be – b2043	0.245 ± 0.008	-	32.2 ± 1.0	3.9	33.4 ± 1.0	4.3
BC07-12		-47.5840	-71.3548	665	310	1.5	24.1815	^{10}Be – b2036	0.207 ± 0.007	-	25.4 ± 0.8	3.1	26.2 ± 0.8	3.3
BC07-43		-47.5079	-71.2451	581	80	1.5	25.7394	^{10}Be – b2055	0.193 ± 0.006	-	25.5 ± 0.8	3.1	26.2 ± 0.9	3.3
outwash terrace														
BC06-32		-47.48563	-71.21694	564	-	3.5	24.1803	^{10}Be – b2074	0.178 ± 0.006	-	24.3 ± 0.8	3.0	-	-
BC06-34		-47.48602	-71.21705	563	-	4	30.9418	^{10}Be – b2075	0.185 ± 0.006	-	25.3 ± 0.7	3.1	-	-
BC06-35		-47.48587	-71.21661	564	-	4	24.7066	^{10}Be – b2078	0.180 ± 0.006	-	24.6 ± 0.8	3.0	-	-
Hatcher[d]														
moraine boulder														
BC07-1		-47.2946	-71.0865	680	95	2	19.6454	^{10}Be – b2049	1.188 ± 0.030	-	139.9 ± 3.6	17.4	170.1 ± 5.3	26.3
BC07-3		-47.2987	-71.0579	673	200	1.5	18.6180	^{10}Be – b1767	1.290 ± 0.037	7.24 ± 0.48	152.8 ± 4.4	19.2	189.6 ± 6.8	30.5
								^{26}Al – a641	*9.545 ± 0.554*		*155.2 ± 10.6*	*24.9*	*226.6 ± 18.3*	*44.4*
BC07-4		-47.2988	-71.0576	678	100	2	20.4468	^{10}Be – b2038	0.952 ± 0.030	6.46 ± 0.41	111.7 ± 3.5	14.0	129.4 ± 4.7	19.1
								^{26}Al – a647	*6.154 ± 0.333*		*109.0 ± 6.0*	*14.9*	*126.0 ± 8.1*	*20.3*
BC07-5		-47.5408	-71.1509	783	135	2	20.0563	^{10}Be – b2039	0.889 ± 0.028	6.52 ± 0.41	95.0 ± 2.9	11.8	107.2 ± 3.7	15.2
								^{26}Al – a649	*5.798 ± 0.319*		*93.3 ± 5.2*	*12.7*	*105.2 ± 6.6*	*16.3*
moraine cobble														
BC06-98		-47.30247	-71.04547	653	-	5	19.6917	^{10}Be – b2087	0.394 ± 0.013	-	47.7 ± 1.5	5.9	-	-
BC06-99		-47.30246	-71.04553	652	-	3	21.2545	^{10}Be – b2080	0.420 ± 0.012	-	50.1 ± 1.4	6.1	-	-
BC06-37		-47.53	-71.14309	762	-	3.5	15.0548	^{10}Be – b1206	0.412 ± 0.020	6.54 ± 0.49	44.0 ± 2.1	5.6	-	-
								^{26}Al – a487	*2.691 ± 0.157*		*42.8 ± 2.5*	*5.7*	-	-
BC06-42		-47.53	-71.14294	763	-	4	15.0285	^{10}Be – b1207	0.526 ± 0.022	5.88 ± 0.41	57.9 ± 2.3	7.3	-	-
								^{26}Al – a488	*3.091 ± 0.171*		*50.5 ± 2.8*	*6.7*	-	-
BC06-43		-47.53	-71.14309	762	-	4	15.5849	^{10}Be – b1208	0.383 ± 0.014	6.75 ± 0.45	41.7 ± 1.5	5.2	-	-
								^{26}Al – a489	*2.587 ± 0.143*		*41.9 ± 2.3*	*5.5*	-	-
Outwash terrace cobble														
S1	BC06-103	-47.2998	-71.0362	620	-	2.5	19.2727	^{10}Be – b2892	1.610 ± 0.043	-	203.7 ± 5.5	25.8	-	-
	BC06-104	-47.2998	-71.0362	622	-	2	25.1177	^{10}Be – b2893	1.832 ± 0.052	-	232.2 ± 6.7	29.8	-	-
	BC06-106	-47.2998	-71.0363	622	-	3	20.9424	^{10}Be – b2896	1.530 ± 0.039	-	193.6 ± 5.0	24.4	-	-
S2	BC07-50	-47.2661	-70.9641	582	-	4	17.4325	^{10}Be – b1772	1.970 ± 0.061	6.35 ± 0.41	265.1 ± 8.4	34.5	-	-
								^{26}Al – a642	*12.51 ± 0.710*		*263.1 ± 16*	*39.1*	-	-
	BC07-51	-47.2661	-70.9642	582	-	2	19.7668	^{10}Be – b2056	1.567 ± 0.043	6.62 ± 0.41	204.0 ± 5.6	26.0	-	-
								^{26}Al – a657	*10.37 ± 0.57*		*209.0 ± 12*	*30.1*	-	-
	BC07-52	-47.2661	-70.9642	582	-	3.5	11.185	^{10}Be – b2037	1.592 ± 0.046	-	210.3 ± 6.2	26.8	-	-
	BC07-53	-47.2661	-70.9642	583	-	2.5	20.107	^{10}Be – b2057	1.932 ± 0.050	6.65 ± 0.46	256.0 ± 6.8	32.9	-	-
								^{26}Al – a658	*12.84 ± 0.82*		*266.9 ± 19*	*40.8*	-	-

Samples processed at the University of Edinburgh's Cosmogenic Isotope Laboratory following procedures adapted from the methods of Bierman et al. (2002) and Kohl and Nishiizumi (1992), for details see supplementary material. Shielding is negligible for all samples (shielding factor <0.9998); rock density 2.7 g cm^{-3} a. All AMS measurements made at S.U.E.R.C. normalised to NIST SRM-4325 Be standard material with a revised (Nishiizumi et al., 2007) nominal ^{10}Be/^{9}Be ratio (2.79 x 10^{-11}) and half-life (1.36 Ma), and the Purdue Z92-0222 Al standard material with a nominal ^{27}Al/^{26}Al ratio of 4.11 x 10^{-11} that agrees with Al standard material of Nishiizumi et al. (2004). Nuclide concentrations include propagated AMS sample/lab-blank uncertainty, 2% carrier mass uncertainty (Be) and 5% stable ^{27}Al measurement (ICP-OES) uncertainty. b. Surface production ratio begins at 6.69. c. Exposure ages calculated using the CRONUS-Earth web based calculator version 2 (Balco. et al 2008) and Dunai (2001) scaling factors. d. Production rate increased by 5% for Hatcher data only by reducing sample air pressure (SL pressure reduced to 1002.3 hPa). e. Erosion rate from Kaplan et al. (2005) at LBA. (int) = internal (analytical) uncertainties; (ext) = propagated external uncertainties (Balco et al. 2008).

Table 3

Click here to download Table: Hein_Table3.doc

Table 3: ^{10}Be data for moraine cobbles on the Moreno I moraine at LBA

Sample ID	Latitude (dd)	Longitude (dd)	Altitude (m asl)	Thickness (cm)	Quartz mass (g)	^{10}Be measured[a] (10^5 atom g^{-1}) (±1σ)
LBA06-1	-46.5645	-70.8851	504	3	14.65	7.30 ± 0.24
LBA06-3	-46.5647	-70.8851	504	3.5	11.69	8.38 ± 0.29
LBA06-5	-46.5649	-70.8850	503	3	11.78	6.74 ± 0.25
LBA06-6	-46.5649	-70.8850	503	4	17.01	7.41 ± 0.39
LBA06-7	-46.5649	-70.8850	504	3	15.70	8.56 ± 0.27

a. All AMS measurements made at S.U.E.R.C. normalised to NIST SRM-4325 Be standard material with a revised (Nishiizumi et al., 2007) nominal ^{10}Be/^{9}Be ratio (2.79×10^{-11}) and half-life (1.36 Ma). Nuclide concentrations include propagated AMS sample/lab-blank uncertainty and 2% carrier mass uncertainty. Shielding is negligible for all samples (shielding factor <0.9998); rock density 2.7 g cm^{-3}.

Figure 1 - color on web only

Click here to download high resolution image

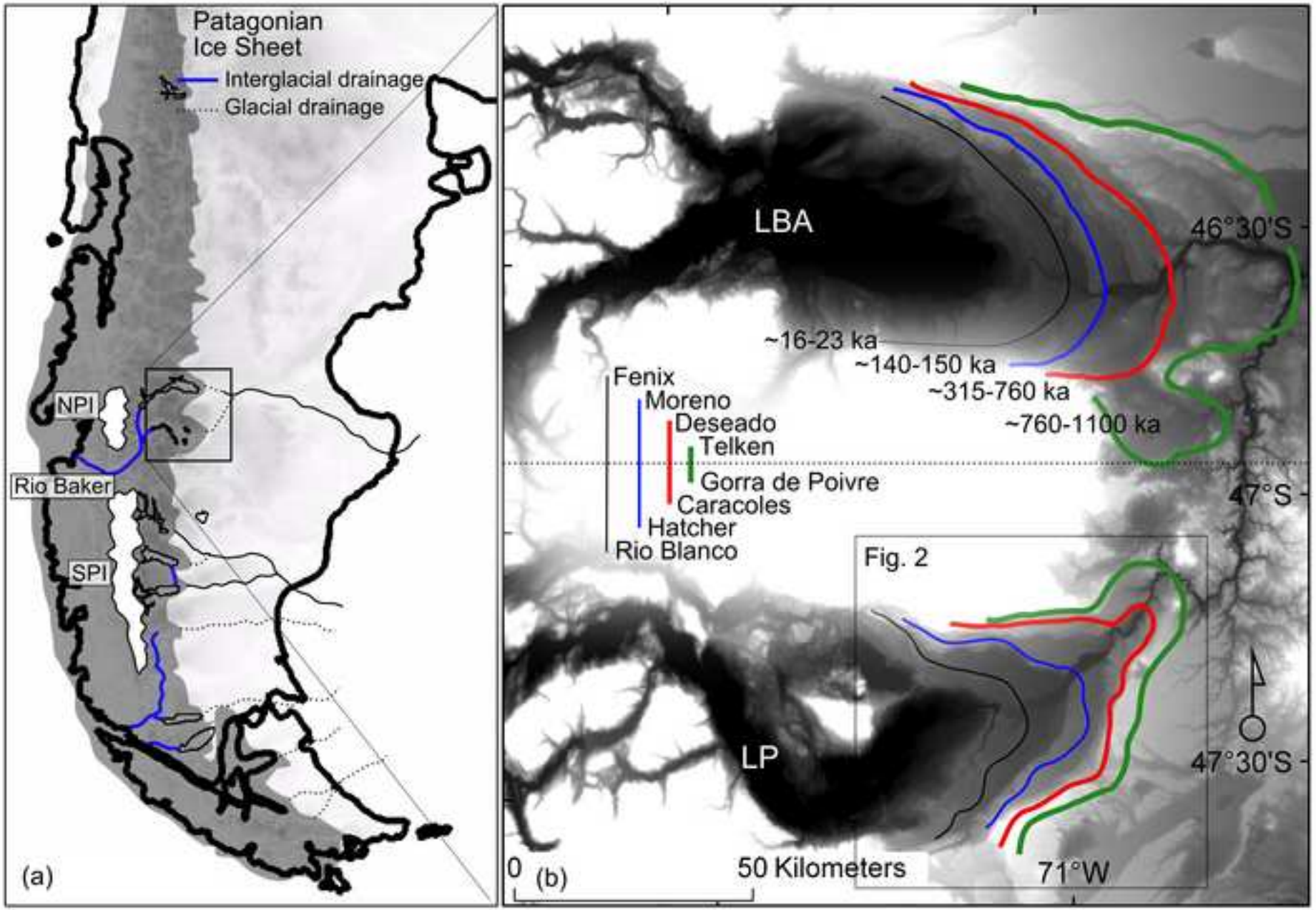

Figure 2 - color on web only

Click here to download high resolution image

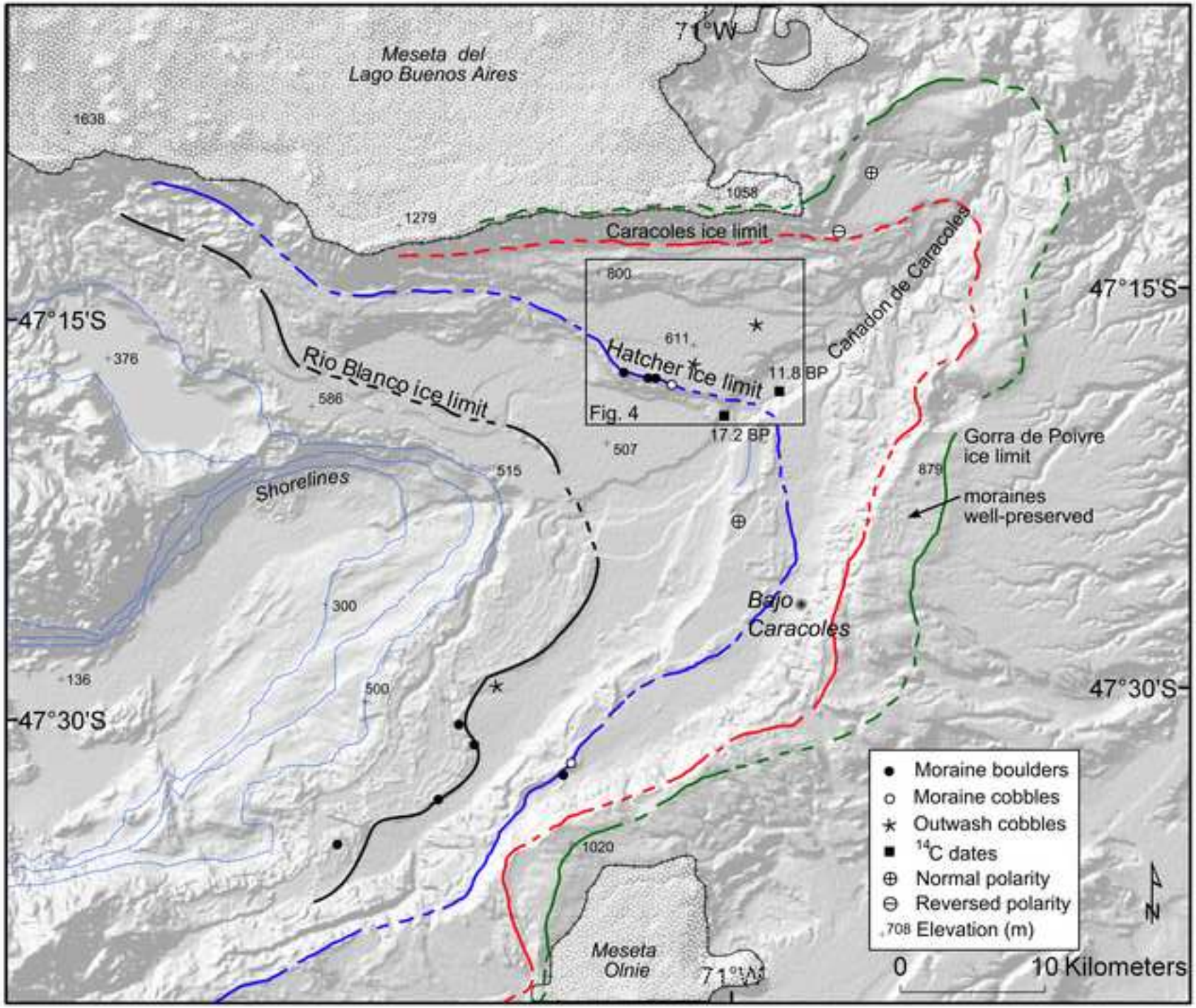

Figure 3 - color on web only

Click here to download high resolution image

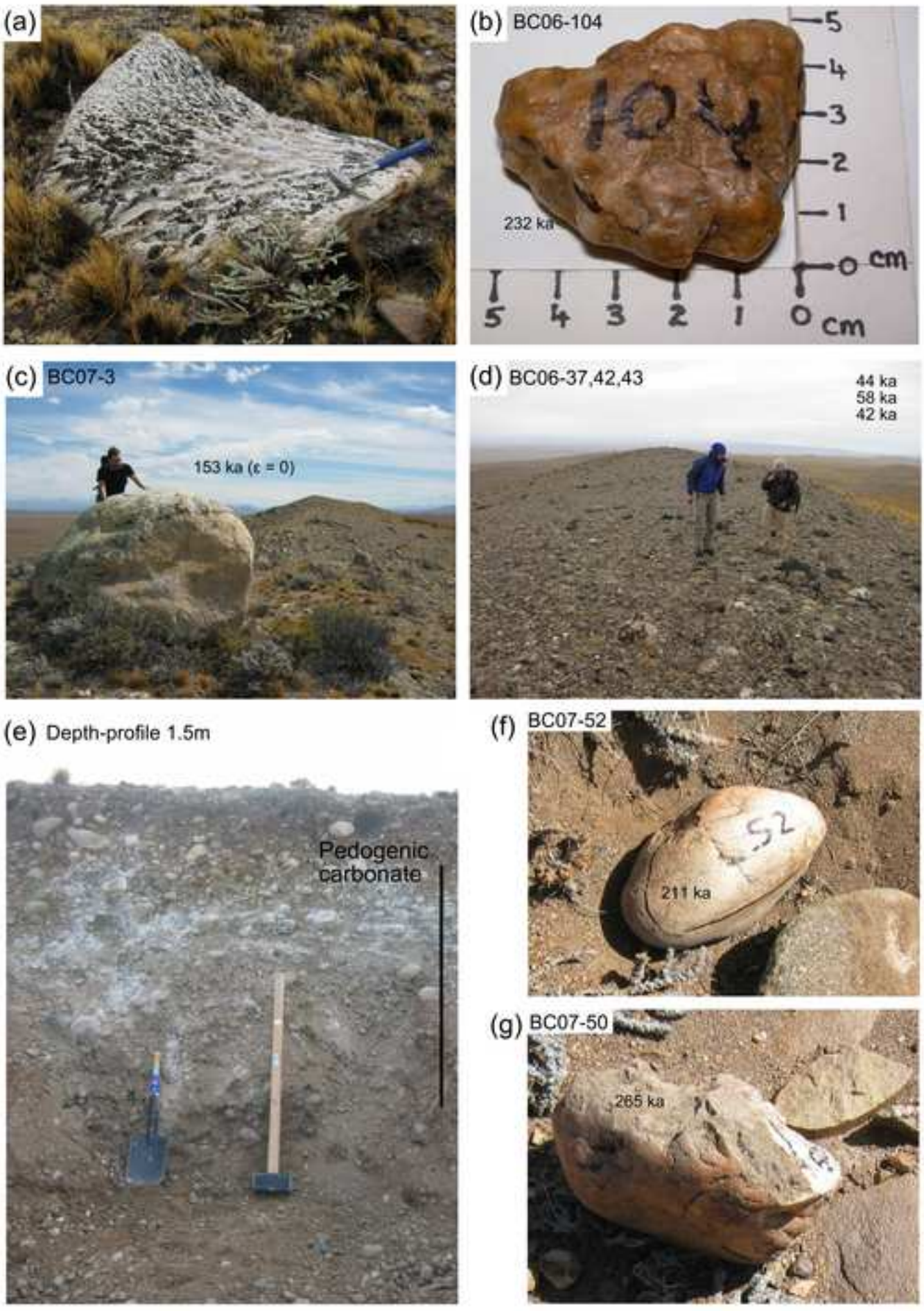

Figure 4

Click here to download high resolution image

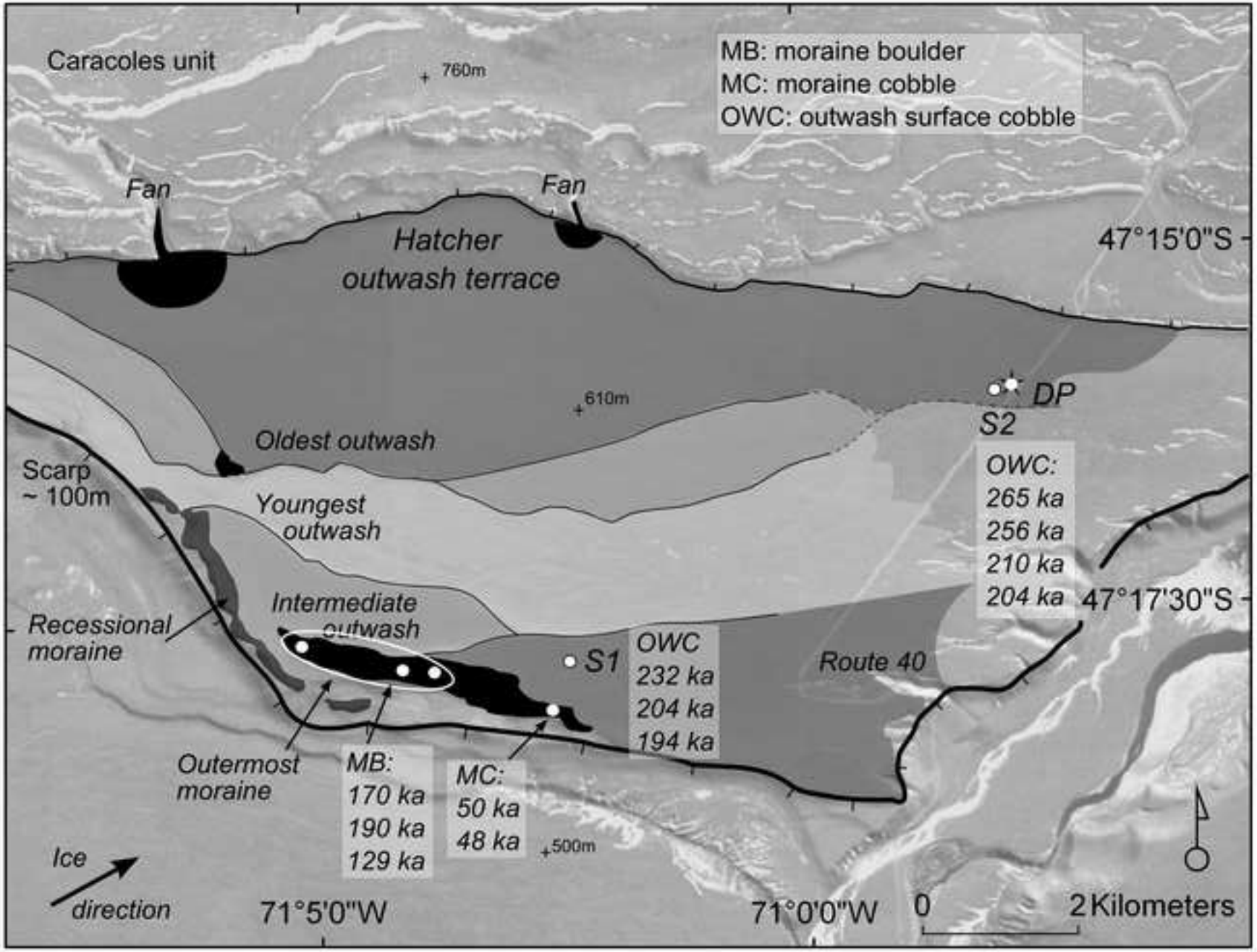

Figure 5 - color on web only

Click here to download high resolution image

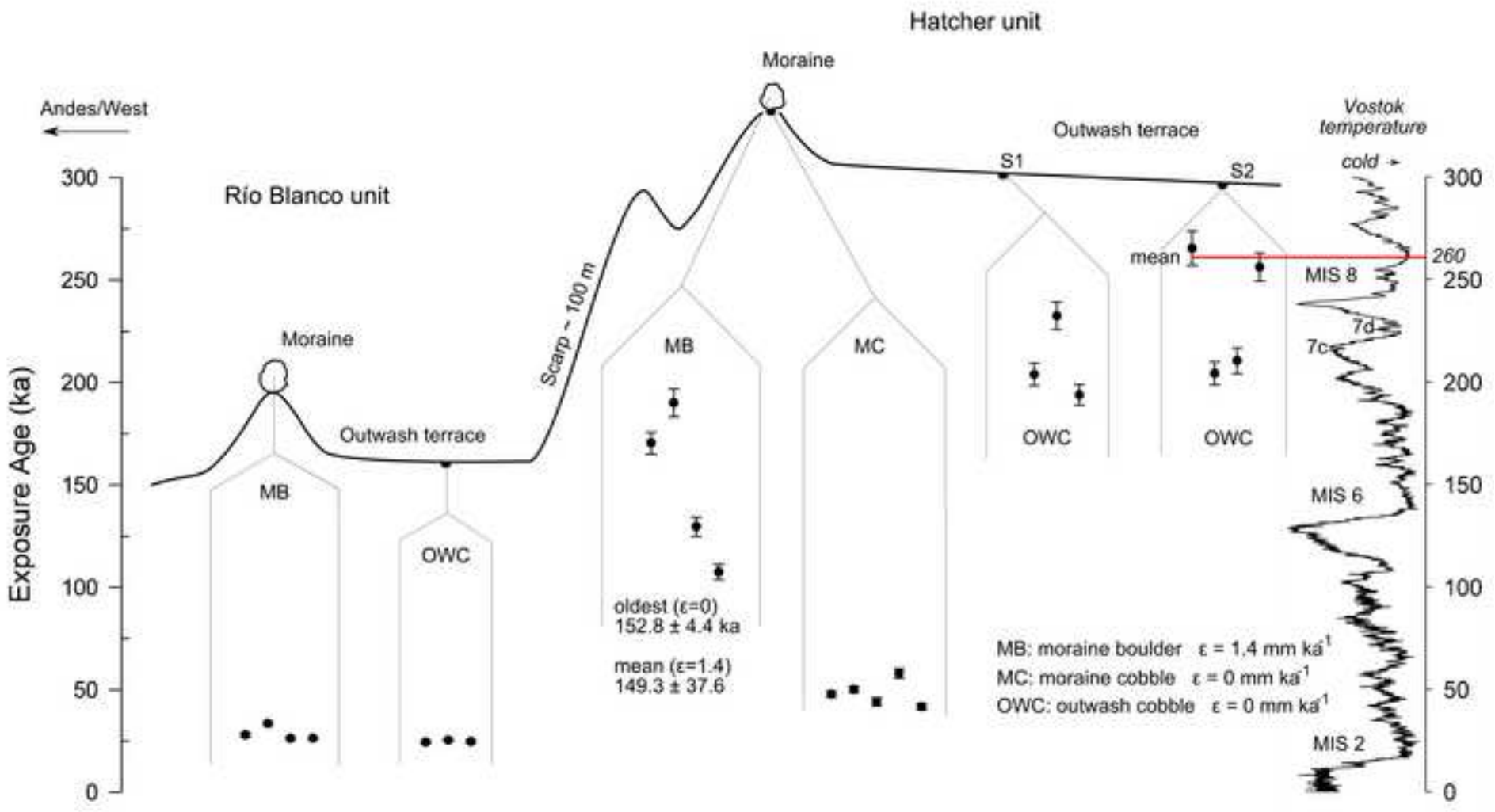

Figure 6a - color on web only

Click here to download high resolution image

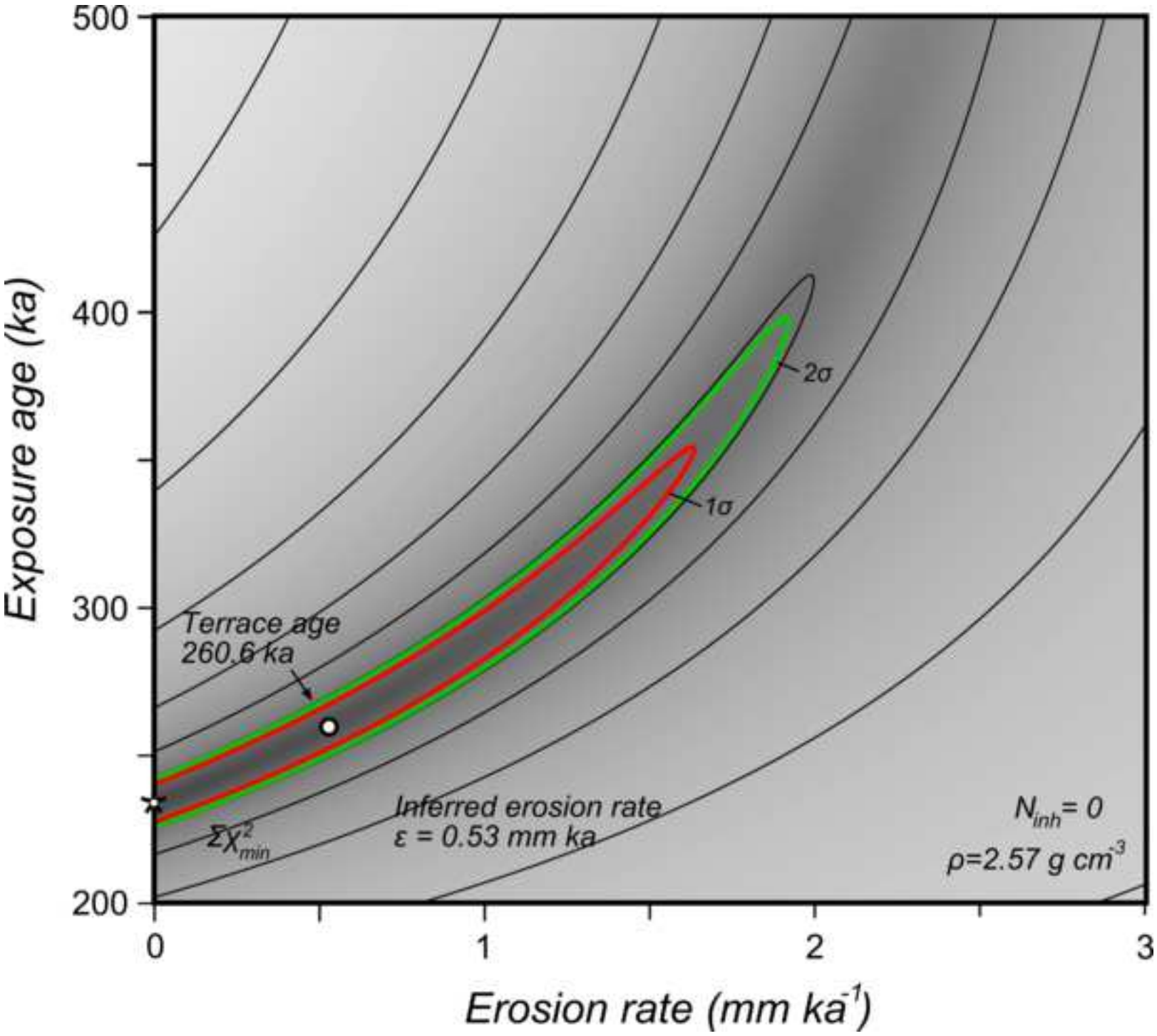

Figure 6b

Click here to download high resolution image

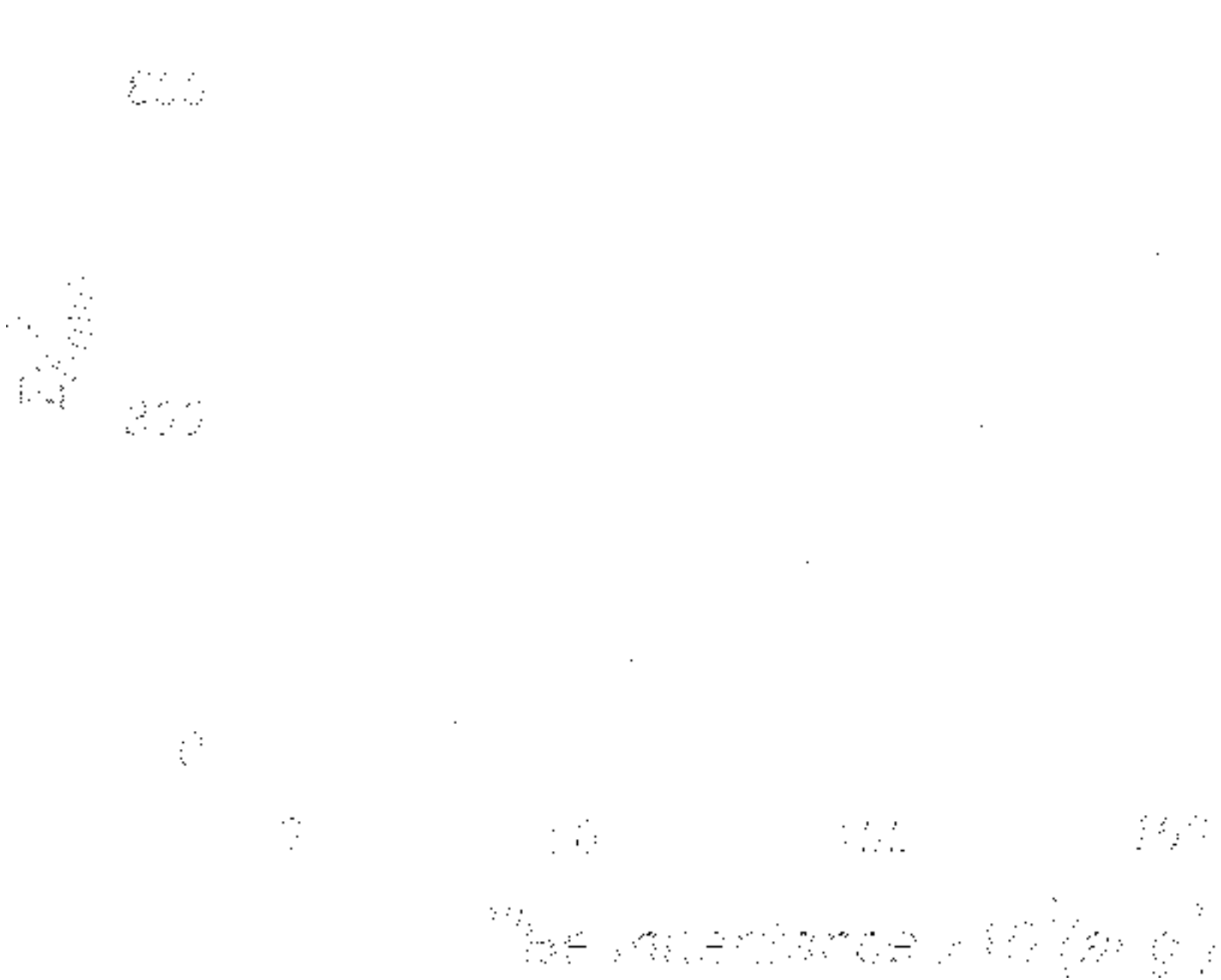

Figure 7a - color on web only

Click here to download high resolution image

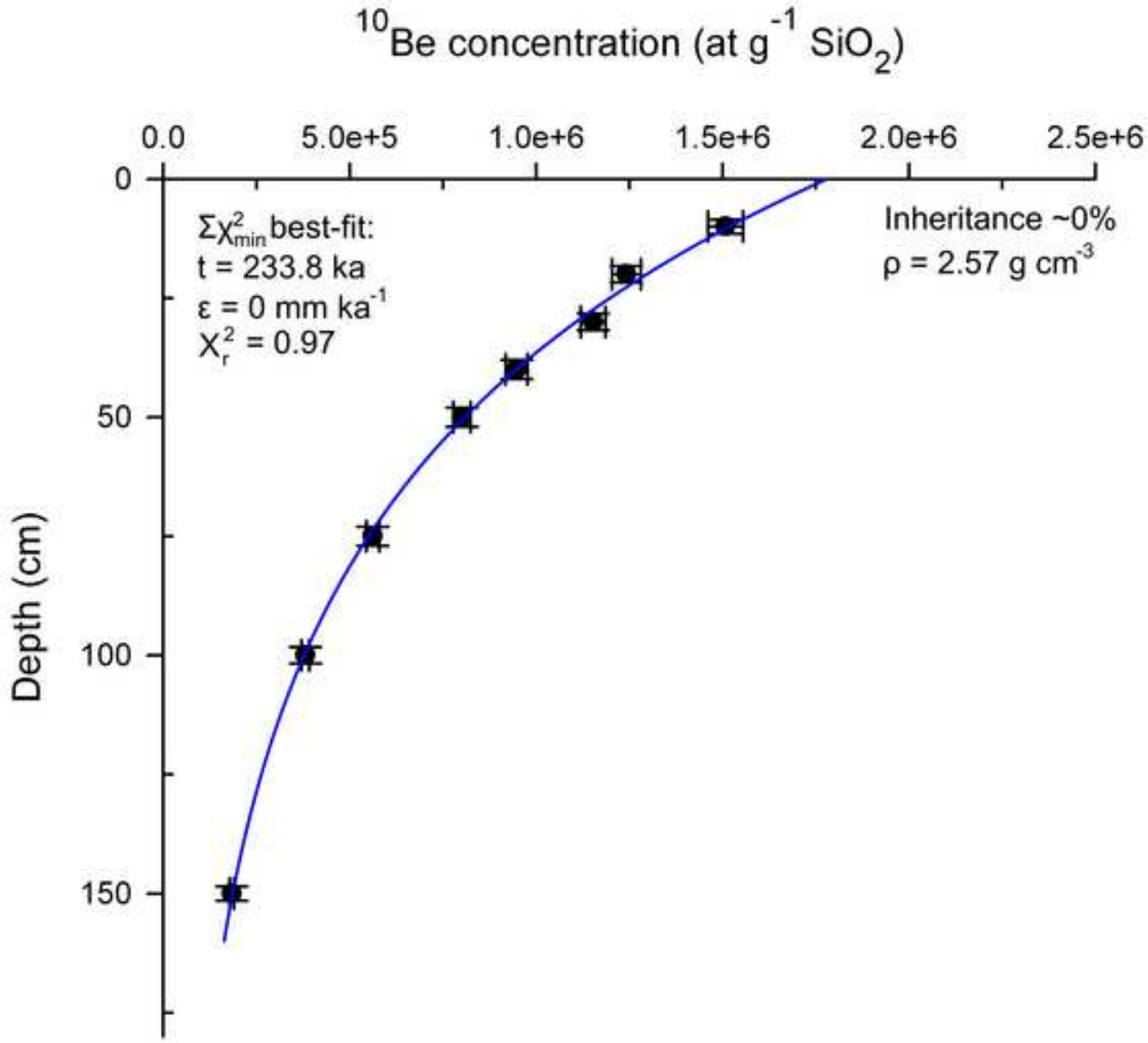

Figure 7b - color on web only

Click here to download high resolution image

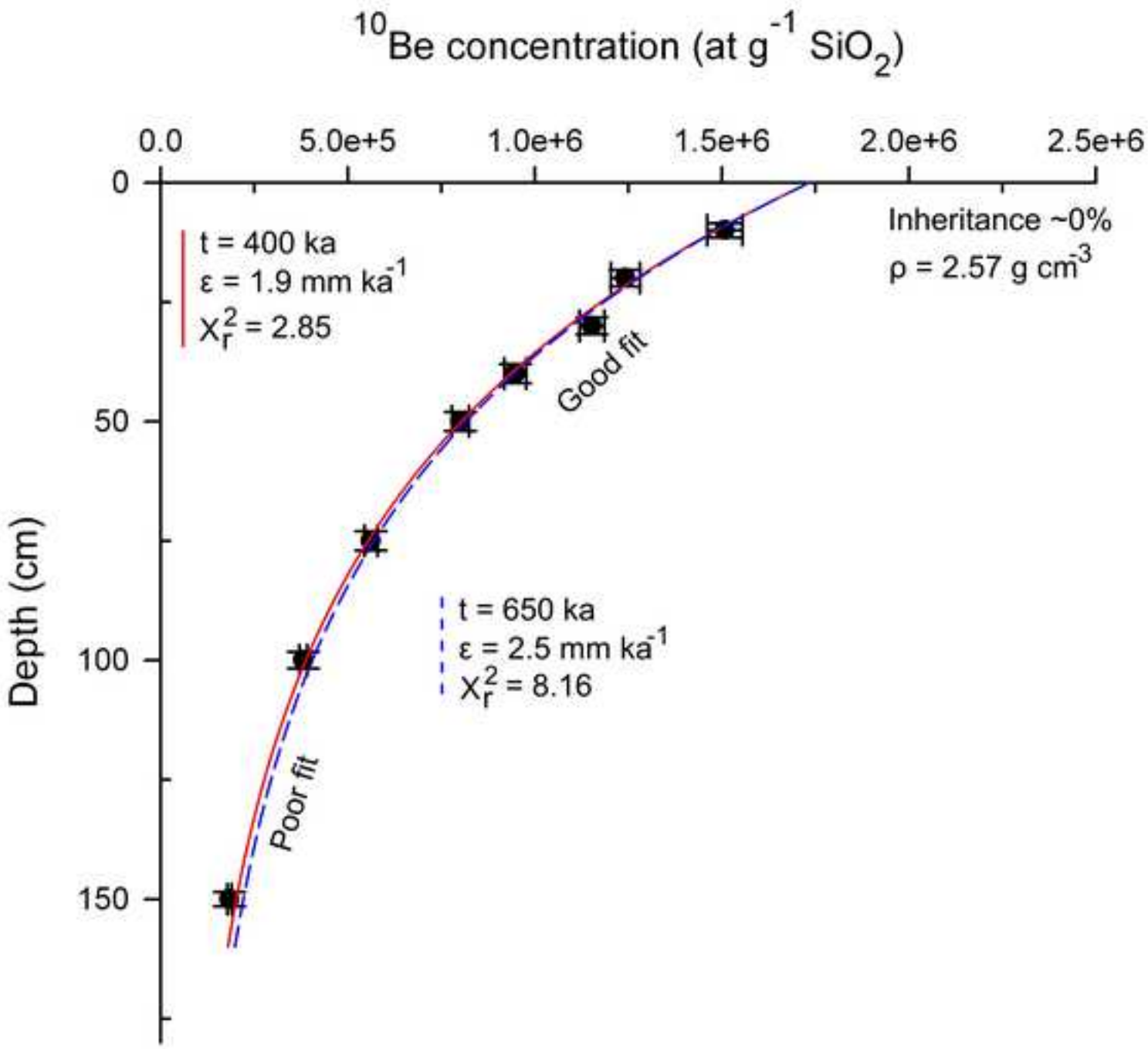

Figure 7c - color on web only

Click here to download high resolution image

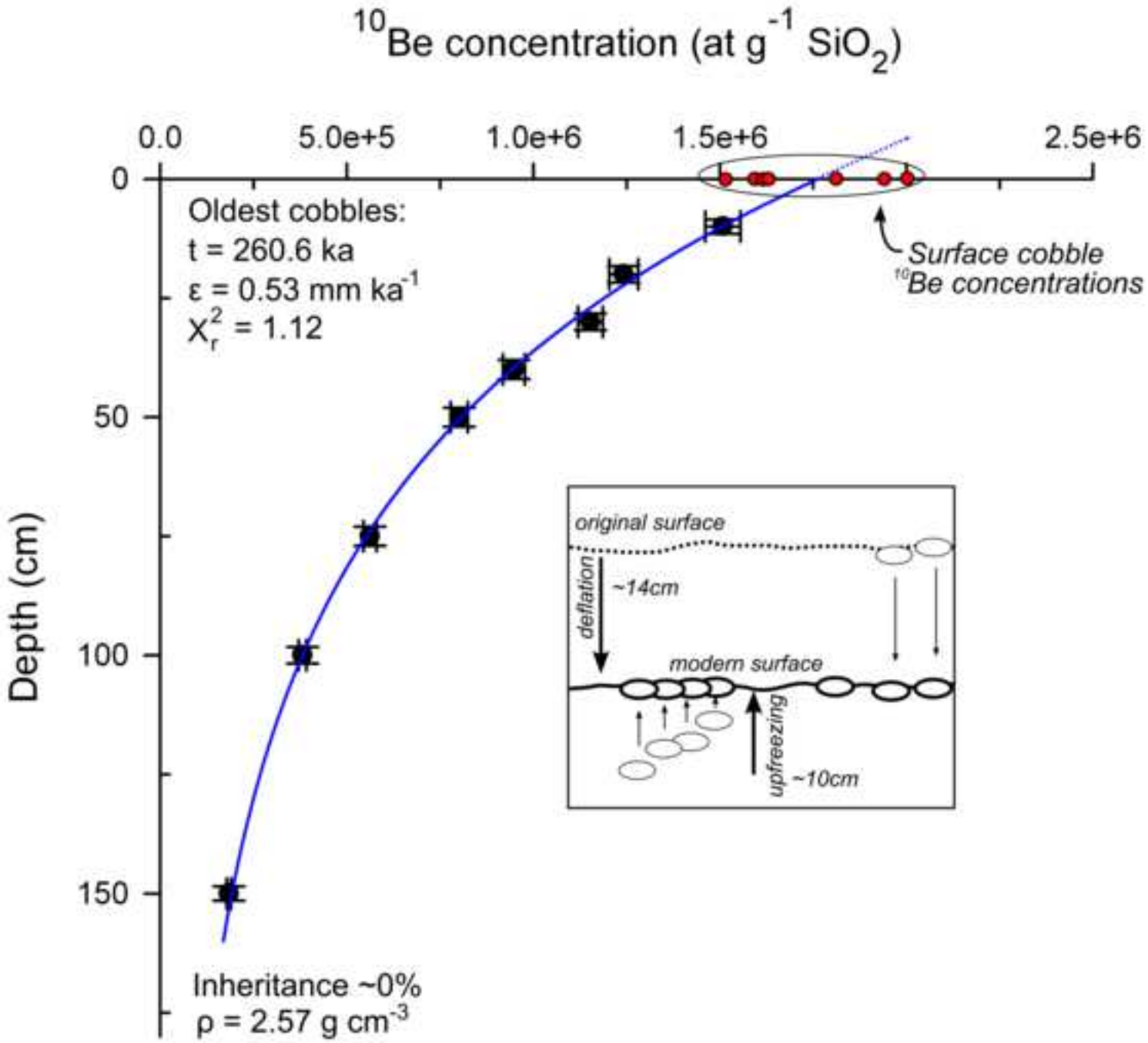

Figure 1 - black and white print version
Click here to download high resolution image

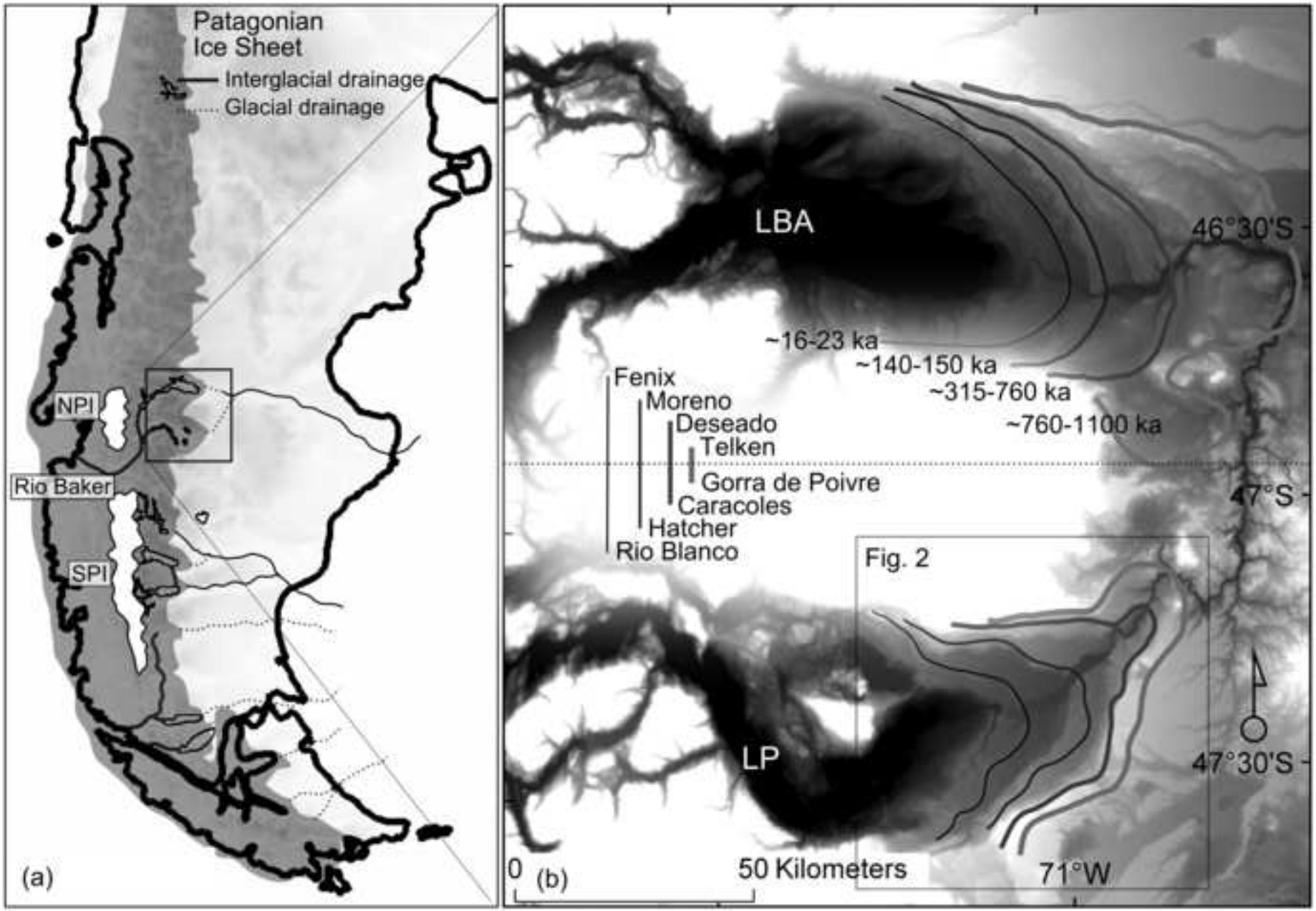

Figure 2 - black and white print version
Click here to download high resolution image

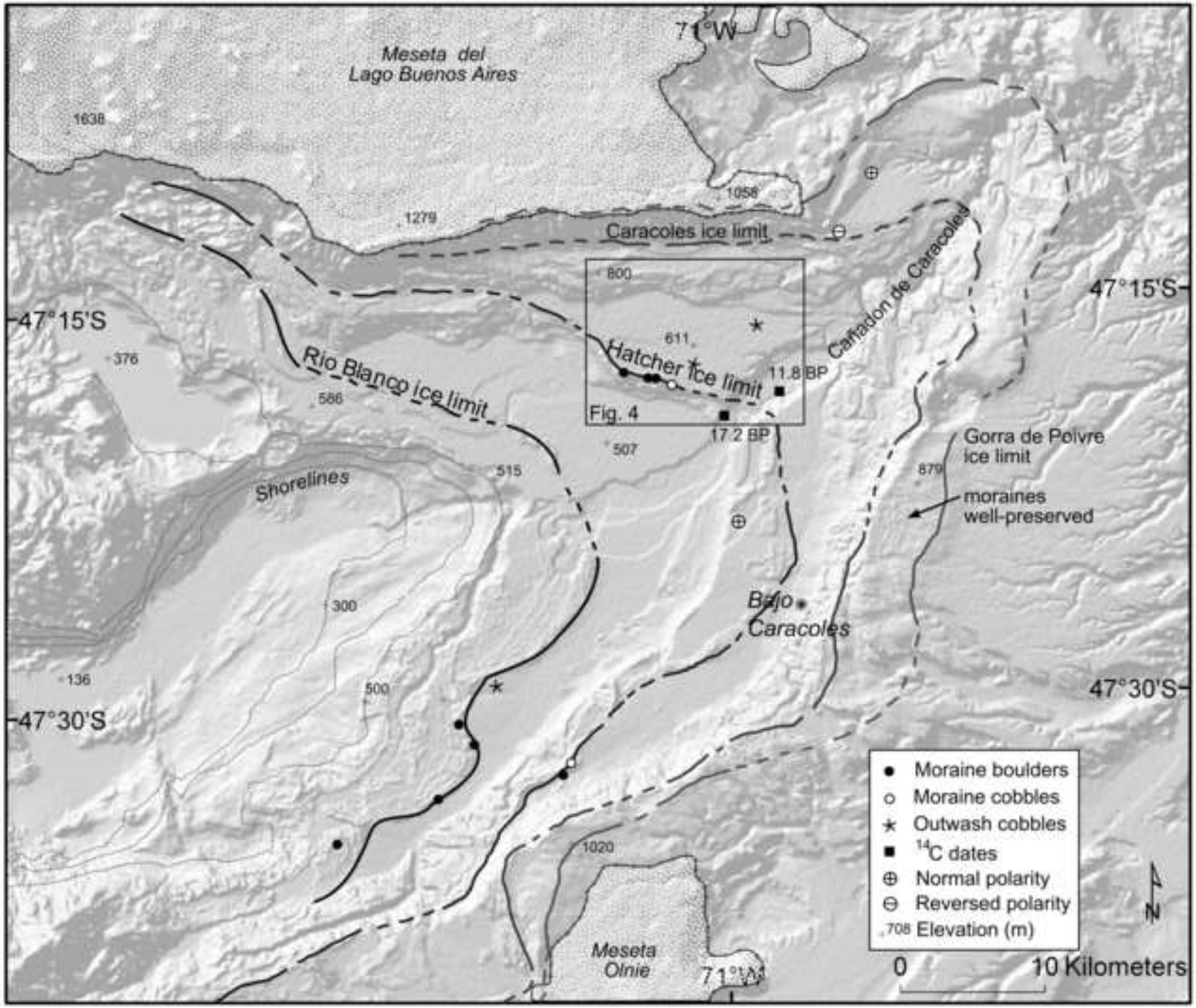

Figure 3 - black and white print version
Click here to download high resolution image

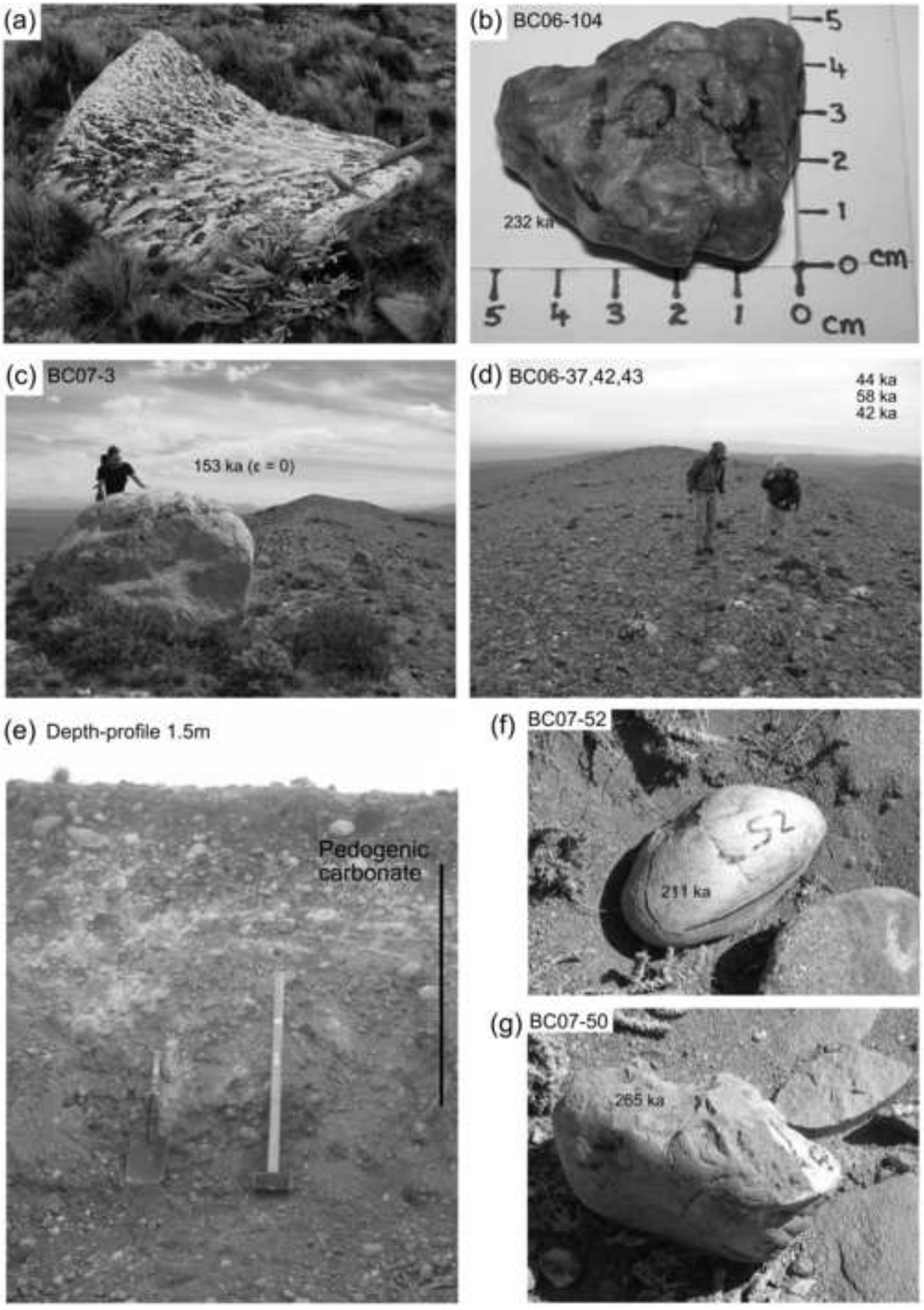

Figure 5 - black and white print version
Click here to download high resolution image

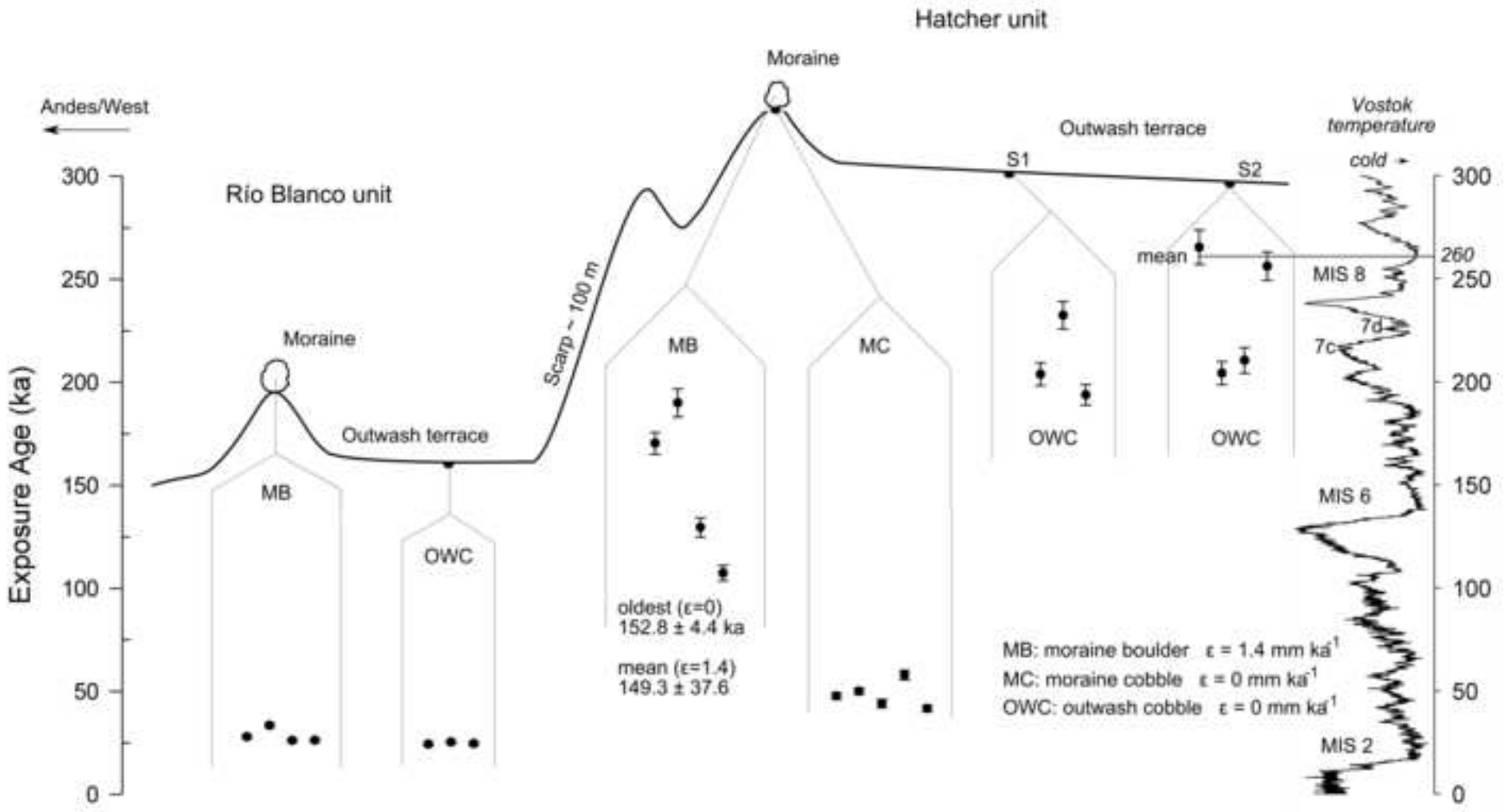

Figure 6a - blackandwhite print version
Click here to download high resolution image

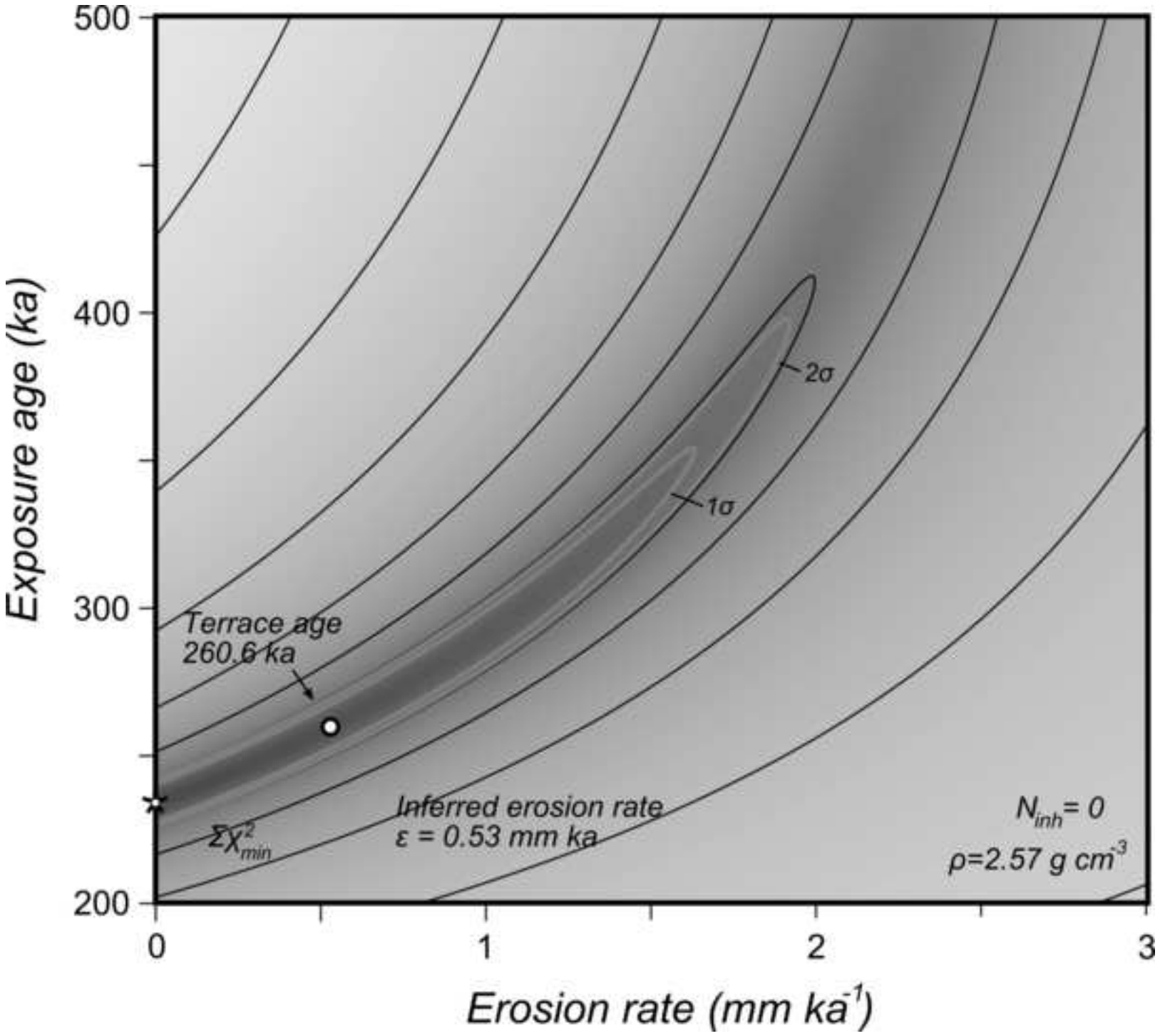

Figure 7a - black and white print version
Click here to download high resolution image

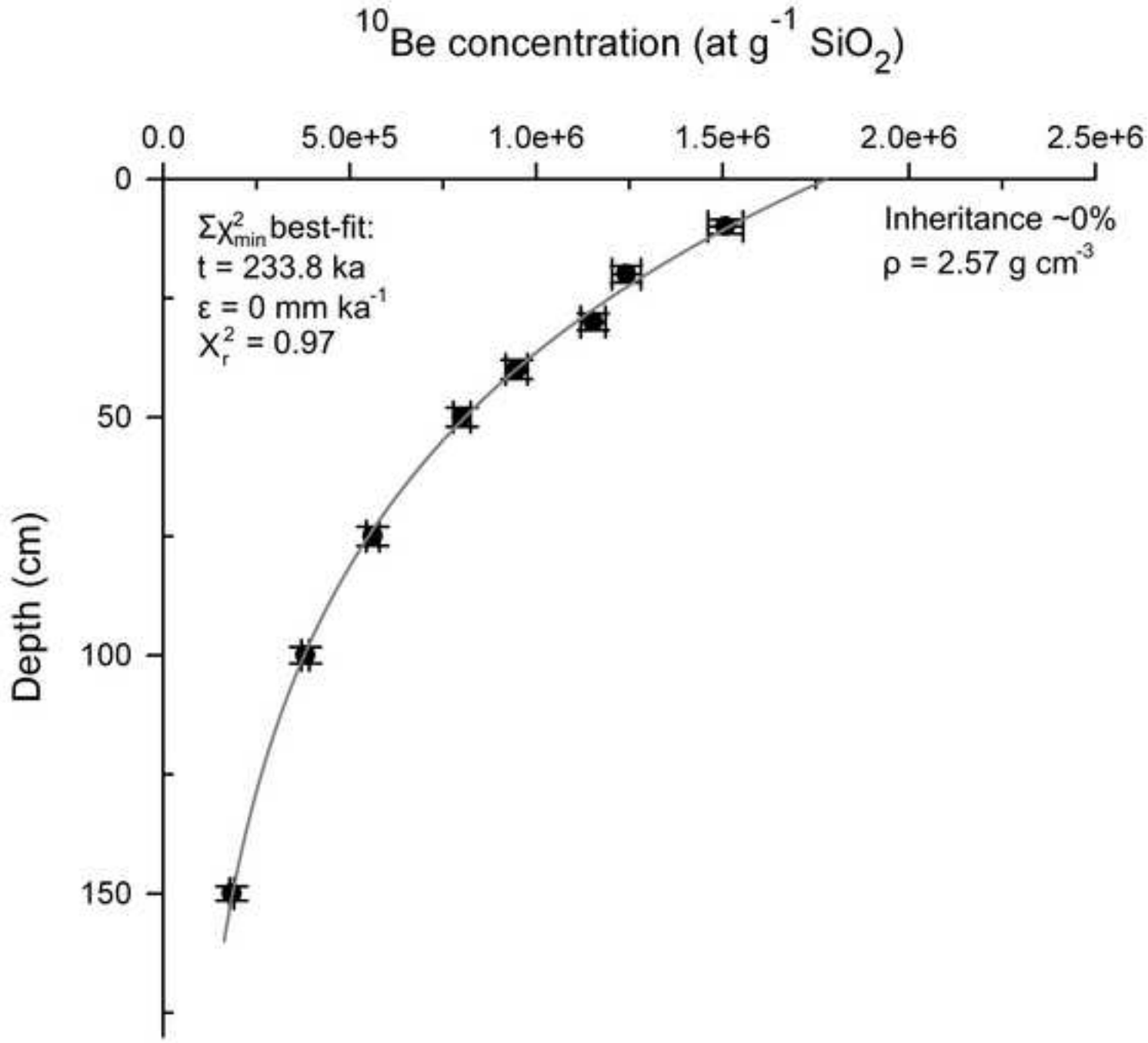

Figure 7b - black and white print version
Click here to download high resolution image

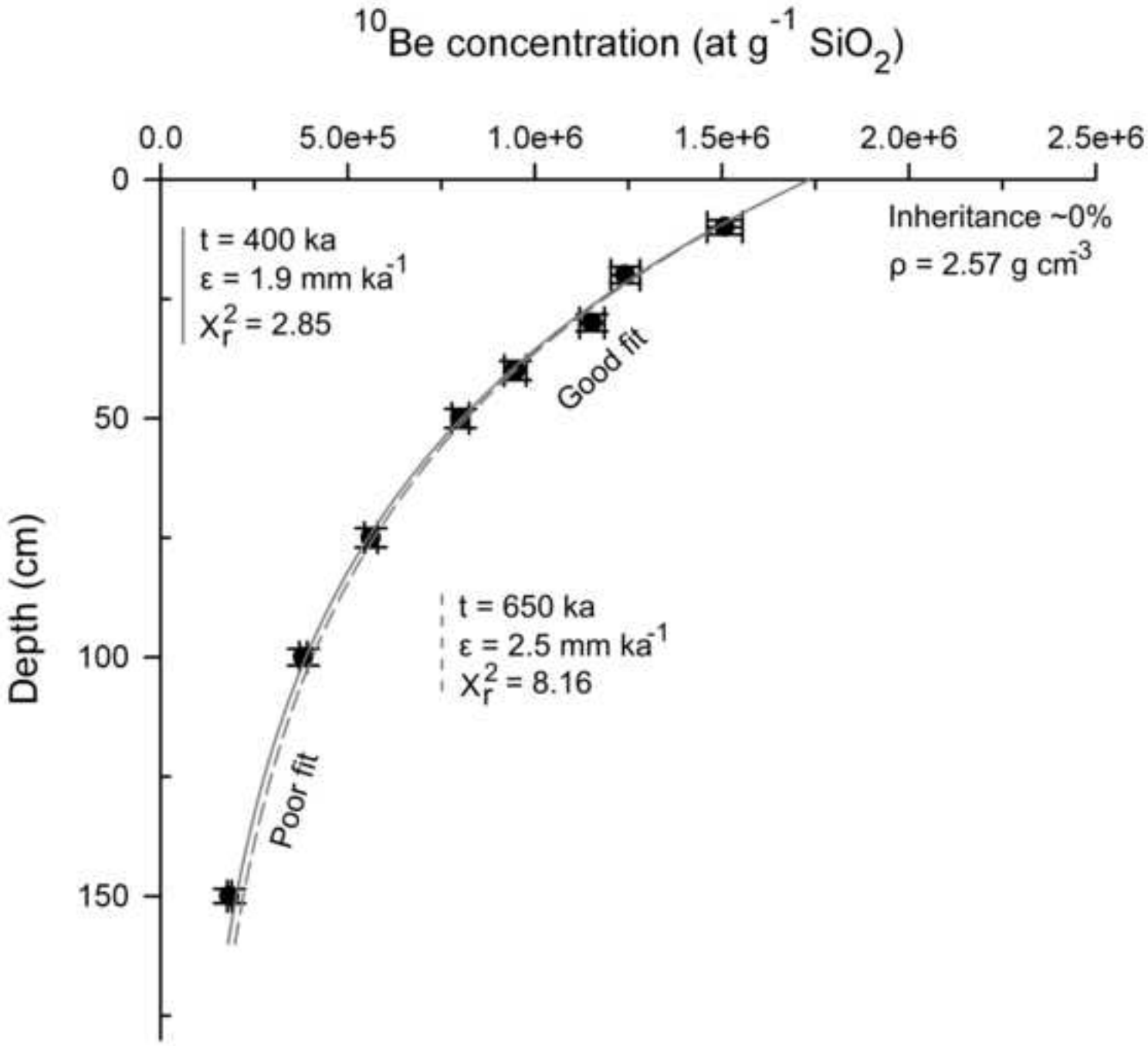

Figure 7c - black and white print version
Click here to download high resolution image